Kinematic Analysis of Planar Parallel Manipulators with Holonomic Higher Pairs

Matthew John D. Hayes

B.Eng. (McGill University), 1995
B.F.A. (Concordia University), 1986

Department of Mechanical Engineering
Centre for Intelligent Machines
McGill University
Montréal, Québec, Canada

August 1996

A thesis submitted to the Faculty of Graduate Studies and Research
in partial fulfilment of the requirements of the degree of
Master of Engineering

Abstract

This thesis presents a detailed kinematic analysis of a 3–degree–of–freedom planar parallel manipulator with holonomic higher pairs. The manipulator consists of a circular disk which rolls without slip on the non–grounded rigid links of each of three 2R serial legs.

The first portion of the thesis is devoted to the review of the geometric and mathematical tools used in the kinematic analysis. *Planar isometries* and *group theory* are used in the development of the inverse kinematics (IK) algorithm. *Kinematic mapping* and *Gröbner bases* are important for the forward kinematics (FK) algorithm.

After six important geometric properties of the manipulator are identified, the IK algorithm is developed. It is based on the decomposability and commutativity of planar displacements. The four step algorithm provides closed form analytic solutions. The algorithm may be used on similar parallel manipulators with any number of 2R legs, and hence, applies to a whole class of manipulators. It will be shown that there can be no more than 4^n real solutions, where n is the number of 2R legs. Three numerical examples are given.

The FK problem is solved using kinematic mapping. To employ a technique from the literature, *pseudo inputs* must be used to specify joint parameter inputs. The resulting set of three non–linear equations in three unknowns is solved using Gröbner bases theory. A numerical example is given.

Finally, velocity and acceleration analysis are performed after the determination of the Jacobian matrix.

Résumé

Le sujet de cette thèse est l'analyse cinématique d'un manipulateur, plan et parallèle, à trois degrés de liberté muni de trois liaisons holonomiques supérieures. La poignée est portée sur trois ou plus pattes à trois liaisons; deux liaisons rotoïdes et une crémaillère. Chaque crémaillère s'engage à un seul engrenage fixé au corps rigide de la poignée et les couples supérieurs sont formées aux points de contact entre les crémaillères et l'engrenage.

On traite, au commencement, la mathématique et la géométrie nécessaires pour l'analyse cinématique. L'algorithme pour la cinématique inverse est basé sur des concepts de la géométrie Euclidienne et non–Euclidienne et de la théorie des groupes. L'algorithme pour la cinématique directe est basé sur des concepts de *kinematic mapping* et de la théorie des *bases de Gröbner*.

Apres avoir identifié six propriétés géométriques importantes, on peut formuler l'algorithme qui conduit à un nombre de solutions analytiques pour la cinématique inverse. Cet nombre des solutions n'excéde pas 4^n, où n est le nombre des pattes sérielles. Afin d'illustrer l'algorithme, on présente des exemples numeriques.

En utilisant le kinematic mapping, les équations de cinématique directe sont obtenues. Les *pseudo entrées* sont nécessaires pour permettre l'utilisation de la méthode développée par Husty. Ces trois équations sont résolues par les calculs symboliques qui utilisent les bases de Gröbner. Finalement, Encore, on présente un exemple.

Enfin, on accomplit l'analyse de vitesse et d'accélération est déduit les matrices Jacobiennes.

Acknowledgements

I am deeply indebted to Professor Paul Zsombor–Murray, my research supervisor, for his challenging suggestions and for his patience in our numerous discussions. His breadth of engineering knowledge and experience, in particular a keen insight of kinematic geometry, along with his constructive criticism throughout the course of this work was instrumental to its completion.

I would also like to warmly thank Professors Manfred Husty (M.U., Leoben) and William O.J. Moser (McGill, Mathematics & Statistics) for their input. The many long discussions I had with them were both enriching and inspiring. Also of great importance was the confidence placed in me by Professors Louis Vroomen, Noriuki Hori and technicians George Dedic and Georges Tewfik (all McGill, Mechanical Engineering).

Special thanks are due to Barbara Whiston for her help in dealing with the myriad administrative details. I also wish to express my gratitude to the members of CIM for their technical assistance.

Of course, the all–too–infrequent informal geometry seminars held at Tompson House with the amicable participation of Doctors Simone Sebben, Peter Hedberg and graduate students Terence (Taz) Ozolins, Kimberly High, Alain Morin, Nabil Elkouh, Stephen Garrioch, Nasrollah Monshi, Gilbert Bande, Stéphan Cyr, Ferhan Bulca, Geoffrey McDowell, David Telfer and Sophia Kounia provided tremendous spiritual fortification.

I am very grateful to my mother and step–father for their eternal support, encouragement and wisdom. I also appreciate the patience and understanding of my

family and friends. The many long hours dedicated to work meant precious short hours for backyard Bar-B-Q's, hockey games, and music making.

Without the pioneering work of Doctors Fredrick Banting and Charles Best this thesis would, quite literally, never have been completed. I especially acknowledge the contribution made by their canine subjects. Doctors Mark Sherman, Stephen Greenberg, Francine Emian along with Mr. Saki Koutelias, Eva Prandekas, R.N., and the rest of the staff at the Royal Victoria Hospital's Metabolic Day Centre are all owed a tremendous debt of gratitude.

I wish to acknowledge the financial support of Doctors Brian Collier, Alan Tenenhouse, Margaret Warner, José Trifaro, and Claudio Cuello and of the Natural Sciences and Engineering Research Council.

Finally, the love and support of Susan Smith was an unfailing source of confidence. Her encouragement was consistent and was indispensable in helping set the stage for the completion of this work. Moreover, she is to be thanked for her tireless proof reading of the manuscript.

To Susan

Table of Contents

List of Figures

List of Tables

Claim of Originality

Certain aspects of the manipulator and its kinematic analysis are original and are presented herein for the first time. The following contributions are of particular interest:

(i) The 3–legged architecture.

(ii) Six "special" geometric manipulator properties.

(iii) An algorithm for the IK problem which results in closed–form solutions.

(iv) The upper bound on the number of IK solutions is 4^n, where n is the number of legs.

(v) The introduction of "pseudo inputs" so a kinematic mapping can be used to solve the FK problem.

Some of the results reported in this thesis have been partly presented in two refereed publications: [**27, 28**].

Chapter 1

Introduction

1.1. Background

This thesis is an investigation of the kinematics of a novel class of planar parallel manipulators. The end effector is a disk which rolls without slip along the straight lines of the non–grounded rigid links of 2R[1] serial legs. Pairs of two 2R serial legs together with the disk form -R-R-G-G-R-R-[2] closed kinematic chains. 2R serial legs may be added as the application requires. Two and three–legged versions will be considered in this thesis (see Fig. 1.1).

A similar manipulator comprised of one closed chain was introduced by Vijay Kumar at the University of Pennsylvania through the work of S.K. Agrawal and R. Pandravada at Ohio University in [**3**]. An analysis of the workspace was made in [**4**], and an attempt to solve the inverse kinematics (IK) problem was made in [**3**]. However, there is a flaw in the IK solution algorithm which may result in erroneous solutions (see Section 1.2).

It is well known that the IK solutions are uncoupled between legs, so solution procedures can treat each leg as a serial chain [**20**]. A result is that a successful IK solution algorithm could be used on platforms with any number of 2R legs. Prior to

[1] An R-pair is a revolute pair.
[2] A G-pair is a higher pair. Details will be presented in section 1.1.1.

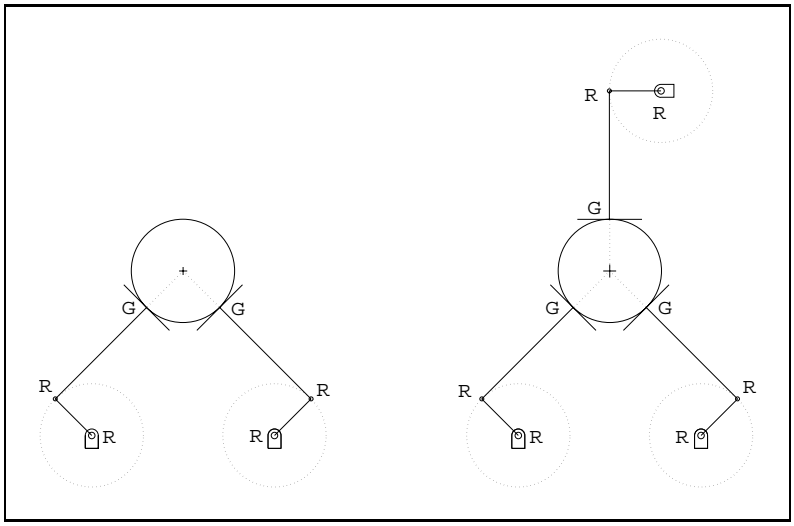

FIGURE 1.1. Two and three–legged planar platforms with higher pairs.

our work, the IK problem reported herein was essentially unsolved, and the forward kinematics (FK) problem had not been addressed.

1.1.1. Lower and Higher Kinematic Pairs. The term *kinematic pair*, or just *pair*, indicates a joint between two links. Joints involving surface contact are called *lower pairs*. Those involving point, line, or curve contact are *higher pairs*. Lower pairs enjoy innate practical advantages. First, applied loads are spread over the contact surfaces, and second, they can be easily and accurately manufactured. There are six types of lower pair, classified as follows [**30**]:

1. **S–pair:** The spherical S–pair consists of a convex or solid sphere which exactly conforms with a spherical shell of identical radius. In other words, a ball–joint. S-pairs have three rotational degrees of freedom (DOF).
2. **E–pair:** The planar E–pair (E stands for the German word *Ebene*, which means plane) is a special S–pair comprising two concentric spheres of infinite radius. To fix one plane relative to the other requires three generalised coordinates, usually two translations and one rotation. Regardless, the E–pair has three DOF.

3. **C–pair:** The cylindrical C–pair consists of mating convex and concave circular cylinders. They can rotate relative to one another, about their common axis, and they can translate relative to each other along that axis. Hence, there are two DOF: one rotational and one translational.
4. **R–pair:** The revolute R–pair is made up of two congruent mating surfaces of revolution. It has one rotational DOF about its axis.
5. **P–pair:** The prismatic P–pair comprises two congruent non–circular cylinders, or prisms. It has one translational DOF whose axis is any straight line parallel to the direction of translation.
6. **H–pair:** The helical H–pair, or screw, consists of two congruent helicoidal surfaces whose elements are a convex screw and a concave nut. For an angle θ of relative rotation about the screw axis there is a translation of distance h in a direction parallel to the screw axis. The sense of the translation depends on the *hand* of the screw threads and on the sense of the rotation. The distance h is the pitch. When $h = 0$, the H–pair becomes an R–pair; when $h = \infty$ it becomes a P–pair. The H–pair has one DOF which is either specified as a translation or a rotation, coupled by the pitch, h.

Any joint that does not fall into these six classifications is a higher pair. A few examples are mating spur gears, a rack and pinion, a cam and follower. These pairs are important because they often offer the simplest means of achieving complex motions. The main drawback is that they are often more complicated, and hence, more expensive to manufacture. The higher pairs may be classified according to the nature of the relative motion between the jointed links:

1. **Pure sliding:** The relative motion is pure translation as in, for example, the finger tip of a robot hand sliding along a flat surface.

2. **Pure rolling:** The relative motion involves rolling without slip. Mating sets of spur gears, and rack and pinion systems are good examples.
3. **Combination of sliding and rolling:** In cam and follower systems the tip of the follower slides along the surface of the cam. As the cam rotates and, relative to the follower, its radius of curvature changes, the follower rotates about some axis. As this occurs the follower tip will also roll on the cam surface.

The subject of this thesis involves higher pairs that roll without slip on a straight line, like rack and pinion gear sets. This type of higher pair will be abbreviated as a **G–pair** (G for gear).

1.1.2. Parallel Manipulators. The recent interest in research and development of robotic systems in general is spurred by the reality of the open market economy wherein goods and services must be sold. A consumer base with diminishing disposable income results in more intense competition among the suppliers. A manufacturer capable of supplying a superior product at a sufficiently high volume and relatively low cost will usually capture a larger share of the market. The ever-growing need for greater efficiency in manufacturing leads to new production methods. Processes that make use of robotic manipulators comprise a large part of these new methods.

Currently, most industrial manipulators have serial architecture. Planar ones, like that shown in Fig. 1.2, have an intermediate link with a degree of connectivity of 2. In other words, an intermediate link of a serial arm is connected to two other links. Terminal links, like the end effector (EE) and base (B), are exceptions. They are jointed to only one other link, and hence, have a degree of connectivity of 1. Serial manipulators have certain advantages because [**16, 25**]:

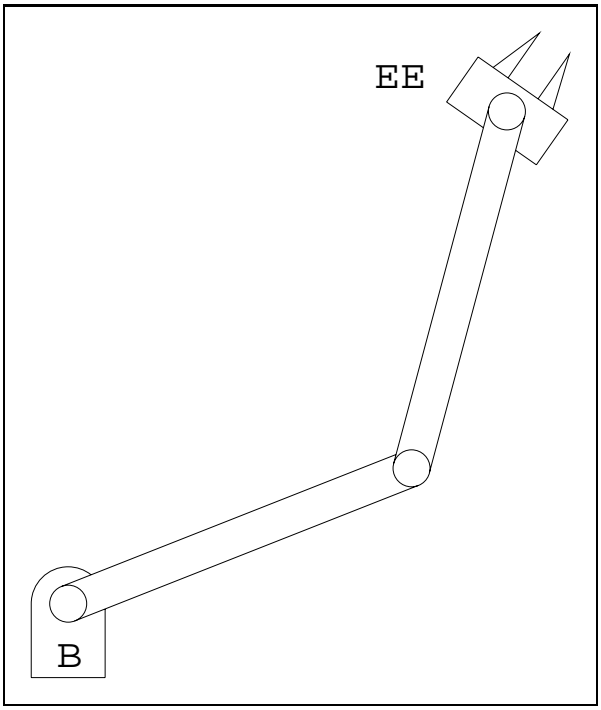

FIGURE 1.2. A planar 3R serial arm.

(i) People can readily identify with an open loop kinematic chain which may be compared with the human arm. This is a strong advantage in programming the arm, training operators, etc..

(ii) Each joint actuator enjoys complete independence.

(iii) The forward and inverse kinematics are well known and the dynamics have been thoroughly analysed for many cases.

It is frequently claimed that serial architecture suffers from the following disadvantages [**25, 20**]:

(i) Serial manipulators require an actuator for each joint. The added mass of the actuators located at intermediate joints contributes to the total inertia of the robot.

(ii) The structural design of the links must take the above point into account. That is, because of the cantilever–like structure of the links, flexibility is a concern.

To control the flexibility of the system the links must be 'over–designed' [**25**]. This usually leads to still more massive links.

(iii) If high degrees of accuracy and precision in motion are required, the velocity of the EE is limited by the above considerations.

(iv) If the actuators are located at the base, force and torque transmission become an issue. Transmission systems reduce the absolute accuracy, precision, and the repeatability of EE motions and add to flexibility.

Therefore, kinematic research turned to parallel architecture in the quest for robot designs that offer more streamlined, cost–effective manufacturing processes. This has led to efforts to develop robots that exhibit better characteristics, e.g., speed of operation, load carrying capacity, dynamic response, accuracy, precision, and reliability. To this end, parallel manipulators consisting of closed kinematic chains have been investigated. Stewart–Gough (SG) type platforms are a typical example, see [**23, 53, 19, 33, 34, 36**]. This type of platform was first devised by Gough [**23**] in 1956 to serve as a test stand for automobile tires. The moving platform is connected to the base by six telescoping prismatic legs. The six legs are jointed to the moving platform, and to the base, by spherical and universal joints. This gives the moving platform 6 DOF. The design was adapted by Stewart [**53**] in 1965 for use as a flight simulator.

Since this thesis is about a particular type of *planar* SG platform consider Fig. 1.3. It depicts a typical planar three–legged SG type platform with nine revolute joints. Note that each 3R serial leg is kinematically equivalent to an -R-P-R- serial leg. This is because a change in location of a reference point on the EE corresponding to changes in the orientation of the first link and the relative angle between the first and intermediate links in the 3R leg can always be achieved by a telescoping -R-P-R- leg. This concept is illustrated in Fig. 1.4. There are many other examples

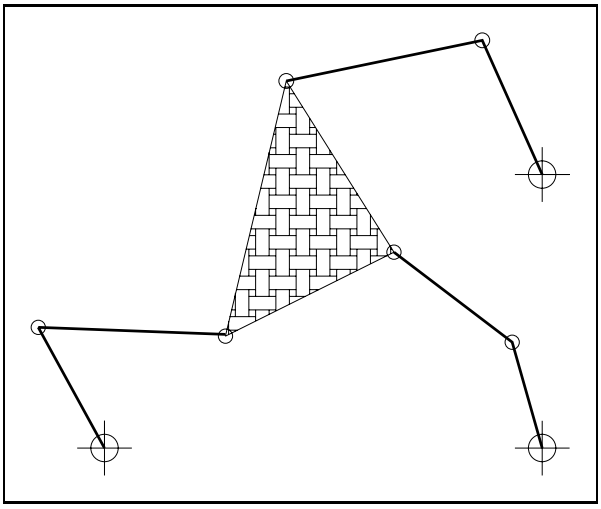

FIGURE 1.3. A typical planar three–legged, 9R SG type platform.

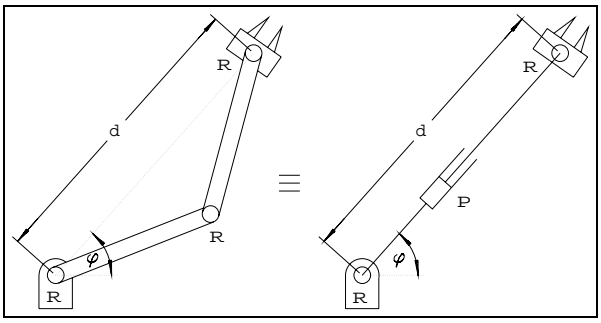

FIGURE 1.4. 3R and -R-P-R- serial chains are kinematically equivalent.

of parallel architecture, see for example [**27, 28, 3, 4, 10, 20, 40, 56**]. Moreover, parallel manipulators have applications in fields other than manufacturing. These include aircraft, ship, and automobile simulators, ambulatory, or walking machines, and robot hands.

Parallel manipulators are characterized by the fact that the EE is attached to the base, or ground, by more than one kinematic chain; an architecture with closed–loops. General advantages of parallel architectures were cited in [**25, 20**]:

(i) It is not necessary for each joint to be actuated directly by individual motors, hence a smaller contribution to the mass of the links. The links, in turn, can be made lighter.

(ii) By allowing at least some motors to be fixed, they can be larger and more powerful. Thus, the load–carrying capacity versus the mass of the robot can be increased, along with the speed of operation.

(iii) The ensuing reduction in gear drives and transmission systems increases the inherent accuracy of the robot while simultaneously lowering the cost to make one.

A few of the potential drawbacks are:

(i) The workspace is limited.

(ii) The workspace may contain many singularities.

(iii) Simultaneous control is required for some or all of the drive motors.

1.1.3. Planar Parallel Systems with Pure–Rolling Higher Pairs. Planar parallel manipulators with higher pairs restricted to pure rolling, such as that shown in Fig. 1.1, constitute an important and unique sub–class. They are important because they have an inherently sound architecture and unique because the pure rolling constraint forces a kinematic dependency on the initial assembly configuration (IAC). That is, displacement analysis requires the presence of initial conditions in the kinematic closure equations. This dependency on the IAC means that analysis is not possible using the conventional techniques employed on lower pair jointed SG type platforms.

1.2. Motivation

Research issues concerning general 3 DOF manipulators form an important sub–group of the problems of manipulator kinematics. Planar 3 DOF manipulators are a special case because the freedoms consist of two linearly independent translations in the plane and rotations about an axis normal to the plane. All planar displacements

belong to the group of isometries of the plane. It is commonly believed that there is no group for general 3 DOF rigid body displacements in space.

The problems of planar manipulators, both serial and parallel, are mostly well documented and understood. Closed form solutions exist for the FK and IK problems of most serial planar manipulators [**16, 42**]. The kinematics of many parallel manipulators are also well understood. For instance, the IK problem of a lower pair jointed SG type platform is identical to the IK problem of a serial manipulator architecturally equivalent to one of each of the kinematic sub–chains of the parallel manipulator [**20**]. On the other hand, the FK problem of parallel platforms is generally more complex than that of serial manipulators. Due to the nature of the problem, much of the earlier research concentrated on numerical solutions [**44, 45**]. While numerical methods are well suited to certain conditions, they yield no insight into theoretical issues, such as the size of the solution space, i.e., the number of assembly modes. Furthermore, these methods rely on an initial guess which must be fairly close to the solution in order to converge [**45, 21**]. Many efforts have been made to provide some theoretical insight by viewing the problem from a different perspective. Gosselin and Sefrioui [**21**] investigated polynomial solutions of the planar SG platform. An algebraic approach was used in [**54**] to derive a degree 6 input–output equation for the same type of platform. Both confirm the well known results of Hunt [**31**].

The success of most of these methods depends largely on the fact that the platforms are jointed with lower pairs. This allows the platform geometry to be readily determined. This is a critical point, since the above methods require knowledge of the platform geometry. However, when the EE is replaced with a disk (pinion gear) and the three revolutes joining the EE to the legs are replaced with racks, along with the condition that contact is always maintained between the racks and pinion,

the geometry suddenly becomes complicated, particularly in the context of the FK problem.

The problem common to all three legged planar platforms with 3 DOF is that, unless redundant actuators are used, only three joint inputs can be specified. The problem unique to the pure rolling contact platform is how the change in location of the contact point between each rack and the pinion affects the displacement. If the pinion remains stationary while a rack moves, it must be that the rack rolls on the disk. Conversely, the pinion can roll on a stationary rack. In the above situations, if the change in location of the contact point along the rack is identical, the displacement of the disk centre will be different. In the first case, the location of the pinion centre is constant. In the second case, it translates along a line parallel to the stationary rack. Most displacements, however, require a combination of the two types of relative rolling. Keeping track of the proportions is critical to both the IK and FK problems. It also appears to be a formidable task. Regardless, all methods thus far depend on the geometry of the platform.

In 1994 a new approach to the kinematic analysis of three legged planar SG platforms jointed with lower pairs was revealed. Husty [**34**] used *kinematic mapping* to solve the FK problem of such platforms. The importance of this approach is that it produces an algorithm which is independent of the platform geometry. Moreover, it was confirmed that there are a maximum of six real solutions using a simple geometric argument [**31**].The same mapping was used to determine the workspace of 3–legged planar platforms in [**35**]. Clearly, kinematic mapping is worthy of study because of its potential as an analytic tool.

The literature on the kinematics of planar parallel manipulators has largely been restricted to manipulators jointed exclusively with lower pairs. The main exceptions being work on rolling contact in the context of grasp and control. Extensive recent

research has been done in connection with grasping and fine–motion manipulation by multi-fingered robotic hands [**40**]. The Utah/MIT dextrous hand is an example. Various types of contact between hand and object have been studied extensively in [**51**]. But, even here the robotic hands are jointed with lower pairs only. The rolling contact is merely an approximation of contact between the EE and workpiece. Continuing in this vein, the kinematics of rolling contact for two surfaces of arbitrary shape were examined in [**12**]. Control schemes for parallel manipulators with rolling constraints were put forward in [**55, 12**]. However, rolling systems are not peculiar to robotic hands. Automatic Guided Vehicles (AGV) are an important class for industrial applications, dangerous materials handling, etc.. The kinematics and dynamics of a three wheeled 2 DOF AGV were studied in great detail in [**49**]. However, in the case of the AGV, continuous rolling contact is a by–product of constraints imposed by the operating environment. It is not a design parameter affecting control (except to detect wheel slip) or kinematic synthesis.

With the exception of cams and gears, which are not considered to be robotic mechanical devices, research on mechanisms containing higher pairs is rare. The roll–without–slip pair is considered in this thesis partly because it can be effectively modelled as a mating gear pair. Gears are common, efficient and reliable machine elements but they are unusual as robotic joints. One intriguing possibility involves the planar parallel systems with the pure rolling higher pairs in Fig. 1.1. If the initial IAC were adjustable then the reachable workspace would be dynamic. This could be accomplished by allowing one rack at a time to disengage and reposition itself on the disk. Such a manipulator has industrial potential.

The effects of the IAC on the reachable workspace of a similar planar rolling system were examined in [**4**]. Previously, the same authors described an algorithm based on vector analysis for the IK problem of the same manipulator [**3**]. However,

they failed to account for the orientation of the end–effector in the inertial reference frame. That is, a relative angle was used to specify the disk orientation, which is a necessary result when a vector approach is employed. The main problem is that there are some displacements where this angle changes, yet the orientation of the end effector remains constant. So, erroneous solutions can arise. No other reference to the IK problem of such a planar manipulator was found. No references, whatsoever, were found in connection with the FK problem of planar parallel manipulators with holonomic higher pairs.

Optimal trajectory planning and obstacle avoidance in a crowded workspace requires fast computation of IK solutions. Control of the robot requires the availability of FK solutions. Hence, this thesis addresses these issues in some detail.

1.3. Thesis Overview

In Chapter 2 the geometry and mathematics relevant to the kinematic analysis used in subsequent chapters will be reviewed. Subjects range from the basic concepts of isometries in the Euclidean plane, which aid in the solution of the IK problem, to the more esoteric notions of kinematic mapping and Gröbner bases, a relatively new tool from computational algebra, for use in solving the FK problem.

Chapter 3 introduces the planar manipulator along with the necessary nomenclature. The mobility is examined and the commutativity of the disk displacements is explained. Finally, six special geometric manipulator properties are given.

In Chapter 4 the development of the IK algorithm is outlined. The four–step algorithm will then be introduced. It is illustrated with three numerical examples.

Chapter 5 contains a discussion of the problems involved in formulating the FK problem. Pseudo inputs are introduced and an adapted version of Husty's algorithm is given, illustrated with a numerical example.

Chapter 6 includes topics beyond static positioning problems. The velocity analysis is necessary for trajectory planning and as the first step in the acceleration analysis. The latter is required for the investigation of manipulator dynamics.

Finally, Chapter 7 contains conclusions and suggestions for future research.

Chapter 2

Mathematical Background

2.1. Isometries

2.1.1. The Group of Isometries of the Euclidean Plane. An isometry of the Euclidean Plane is a one–to–one mapping of the plane onto itself which leaves distance invariant. The isometries consist of rotations, translations, reflections, and glide reflections. They are congruent transformations that are also called *motions of the plane* [**14**]. However, the use of the term *motion* is misleading. An isometry of the plane is the correspondence between the initial and final positions of an object in the plane displaced in a way that leaves the distance between every pair of points in the object unchanged. Although a motion takes place, the motion is not the isometry. A motion is a continuous series of infinitesimal displacements.

Planar isometries constitute a *group*. A group consists of a set, $\mathcal{G}$, together with a binary operator, $*$, defined on $\mathcal{G}$ which satisfies the following axioms [**7**]:

1) [closure]	$x * y \in \mathcal{G}$	$\forall\ x, y \in \mathcal{G}$
2) [associativity]	$(x * y) * z = x * (y * z)$	$\forall\ x, y, z \in \mathcal{G}$
3) [identity]	$\exists\ I \in \mathcal{G}$:	$I * x = x * I = x$, $\forall\ x \in \mathcal{G}$
4) [inverse]	$\exists\ x^{-1} \in \mathcal{G}$:	$x * x^{-1} = x^{-1} * x = I$, $\forall\ x \in \mathcal{G}$

If in addition to axioms 1) through 4), the elements in $\mathcal{G}$ are commutative (i.e., $x * y = y * x, \forall x, y \in \mathcal{G}$) then $\mathcal{G}$ is an *Abelian*, or *commutative* group. The Abelian group axioms of *closure* and *commutativity* will prove to be indispensable in the development of a solution procedure for the IK problem.

2.1.2. The Sub–Group of Direct Isometries. A subset of $\mathcal{G}$ which is a group under the binary operator defined on $\mathcal{G}$ is a sub–group $\mathcal{H}$ [**9**]. It is well known [**14**] that the isometries of the plane are a group. Let $\mathcal{I}$ be this group. A planar displacement consists of the direct isometries only. The direct isometries are translations and rotations. Let $\mathcal{D}$ be the sub–group of planar displacements of group $\mathcal{I}$. The manipulator under study has 3 DOF. Two are translations in the directions of the basis vectors of a non–moving reference frame (the inertial reference frame), the third consists of rotations about the centre of the disk. The group operator in $\mathcal{D}$, called "product", is denoted by the symbol $*$. It represents successive implementations of given isometries and hence is not an algebraic product. By virtue of the axiom of closure, all the products of all translations and all rotations are also in $\mathcal{D}$. Hence, the disk can move in any combination of translation and rotation within the physical limits of its workspace.

Since direct isometries preserve sense, as well as distance, the product of any number of direct isometries is another direct isometry. It is easy to show that the associativity axiom holds for the product of three direct isometries. It is equally simple to show the existence of an identity displacement and that there is an inverse for every displacement in the plane. Hence, $\mathcal{D}$ is indeed a sub–group of $\mathcal{I}$. However, the indirect, or opposite, isometries do not preserve sense and therefore do not form a sub–group since the product of opposite isometries is not necessarily opposite. For example, the product of two reflections in parallel lines is a translation through twice the distance between the lines. The product of two reflections in intersecting lines is

a rotation through twice the angle between the lines. In both cases, the product of two opposite isometries is a direct isometry. Since direct isometries are not opposite, closure is violated, hence the opposite isometries do not form a sub–group of $\mathcal{I}$.

2.2. Projective Geometry

2.2.1. Five Axioms. Some concepts from projective geometry are introduced here primarily to provide background for the kinematic mapping, which is later used to solve the FK problem. Kinematic mapping involves the transformation of given displacement parameters from the Euclidean plane to a three dimensional projective image space.

The following axioms are extracted from Euclidean geometry [**5**]:

(1): Any two distinct points determine one and only one line.

(2): Any three distinct non–collinear points, also any line and a point not on the line, determine one and only one plane.

(3): Two distinct coplanar lines either intersect in a point or are parallel.

(4): A line not in a given plane either intersects the plane in a point or is parallel to the plane.

(5): Two distinct planes either intersect in a line or are parallel.

Note that these propositions deal only with the connection of points and the intersections of lines and planes. They are entirely free of metric notions.

The space in which projective geometry operates is constructed by expanding Euclidean geometry. That is, certain objects are adjoined to the Euclidean plane and space. These objects are the *ideal points, lines* and *planes*. For purposes of distinction, let the Euclidean counterparts be called *ordinary*. The last three of the previously stated five axioms from Euclidean geometry are amended such that they

hold true for all combinations of ideal and ordinary quantities. The space that results is called *projective space*.

(1'): Any two distinct points determine one and only one line.

(2'): Any three distinct non–collinear points, also any line and a point not on the line, determine one and only one plane.

(3'): Any two distinct coplanar lines intersect in one, and only one point.

(4'): Any line not in a given plane intersects the plane in one, and only one point.

(5'): Any two distinct planes intersect in one, and only one line.

Consider first the projective plane, P^2. The ordinary lines are adjoined with an ideal point (called the *point at infinity*) to become projective lines. Two distinct intersecting ordinary lines will have distinct points at infinity. Two ordinary parallel lines will share the same point at infinity. The ordinary plane together with the totality of the points at infinity of its ordinary lines constitutes the projective plane, P^2. A projective line has but one point at infinity, not two (one for each direction). That is, a projective line is *closed*, this idea is discussed at length in subsection 2.2.2. Also, all the points at infinity of a given projective plane lay on the same line at infinity.

Projective space, P^3 consists of the totality of projective planes. The lines at infinity associated with each plane in the projective space are coplanar. The plane in which they lie is called the *plane at infinity*.

2.2.2. Homogeneous Coordinates. Let O be the origin of the Cartesian coordinate system, $\{O : x, y\}$ shown in Fig. 2.1. Let Q be a distinct point in the plane. The ray passing through O and Q is described by $Q(\mu x, \mu y)$, where $\mu \in \mathcal{R}$ (ie., a real number). Conversely, for a given point $S \neq O$ the pair $(\mu x, \mu y)$ describes

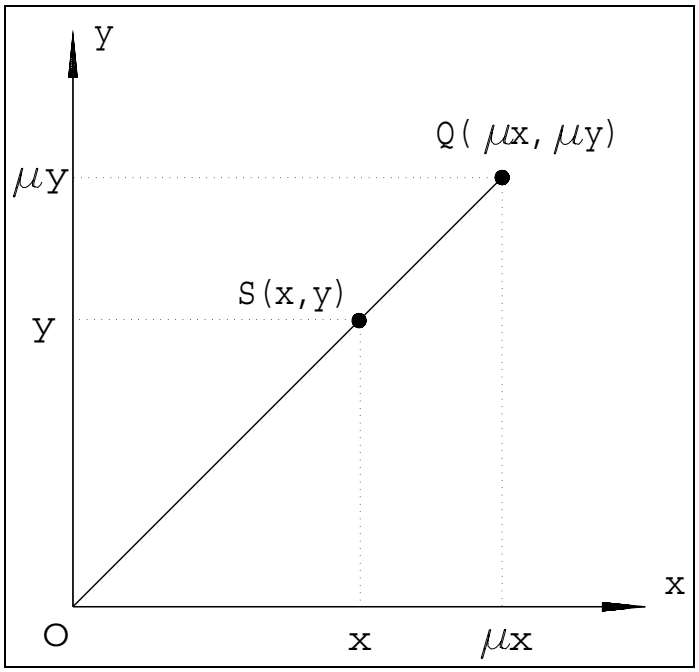

FIGURE 2.1. Cartesian coordinates in E^2.

a distinct point Q on OS. As $\mu \to \pm\infty$ the seemingly meaningless pair (∞, ∞) is obtained.

If $S = (x, y) \in E^2$ and (x_1, x_2, x_h) is an ordered triple with $x_h \neq 0$, then the point S can be uniquely described by the triple if the point S is represented as:

$$x = \frac{x_1}{x_h} \quad , \quad y = \frac{x_2}{x_h}. \tag{2.2.1}$$

Then any triple of the form $(\lambda x_1, \lambda x_2, \lambda x_h)$ (for $\lambda \neq 0$) describes exactly the same point S. In other words, two real points are equal if their homogeneous coordinates are proportional. This is because

$$\frac{\lambda x_1}{\lambda x_h} = \frac{x_1}{x_h} = x, \quad \text{and} \quad \frac{\lambda x_2}{\lambda x_h} = y.$$

The coordinates $(x_1 : x_2 : x_h)$ are called *homogeneous coordinates*, where x_h is the *homogenizing* coordinate. Note that when $x_h = 1$ the Cartesian coordinate pair (x, y) is recovered.

The Cartesian coordinates $(\mu x, \mu y)$, $\mu \neq 0$, of the family of points on the ray through Q in Fig. 2.1 can be expressed in homogeneous coordinates as follows:

$$(\mu x, \mu y) = (\mu x_1 : \mu x_2 : x_h) = (x_1 : x_2 : \frac{x_h}{\mu}).$$

In E^2, as $\mu \to \pm\infty$ the homogeneous coordinates $(x_1 : x_2 : 0)$ are obtained. There is no point on the line OS to which this triple can correspond because E^2 is unbounded. In the extended Euclidean plane the triple $(x_1 : x_2 : 0)$ describes the *point at infinity (ideal point)* on the line OS. Since the same triple is obtained regardless if $\mu \to +\infty$ or $\mu \to -\infty$, a single, unique point at infinity is associated with the line OS in E^2. Hence, an ordinary line adjoined by its point at infinity is a closed curve.

The triple $(0 : 0 : 0)$ describes neither an ideal point or a real point on OS. $(x : y : 0) = (0 : 0 : 0)$ seems to imply that $S = O$, which is a contradiction in the construction of the line segment OS. The trivial triple $(0 : 0 : 0)$ is therefore discounted.

Entirely analogous statements can be made for the three-dimensional Euclidean space, E^3. This space is covered by a *Cartesian coordinate-system* $\{O : x, y, z\}$ with the origin O and axes x, y, z. The axes are usually defined as orthogonal. Such an orthogonal Cartesian system is illustrated in Fig. 2.2. As Fig. 2.2 shows, a unique triple, (x, y, z) can be assigned to every point $S \in E^3$. The converse is also true. A point $Q \in l = OS$ has the coordinates $Q(\mu x, \mu y, \mu z)$, where $\mu \in \mathcal{R}$. As $\mu \to \pm\infty$ the triple (∞, ∞, ∞), is obtained.

The projective homogeneous coordinates $(x_1 : x_2 : x_3 : x_h)$ of the point $S \in E^3$ are defined as:

$$x = \frac{x_1}{x_h}, y = \frac{x_2}{x_h}, z = \frac{x_3}{x_h} \quad , \quad x_h \neq 0. \tag{2.2.2}$$

As in two dimensional projective space, when $x_h = 1$ the Cartesian coordinate triple (x, y, z) is recovered.

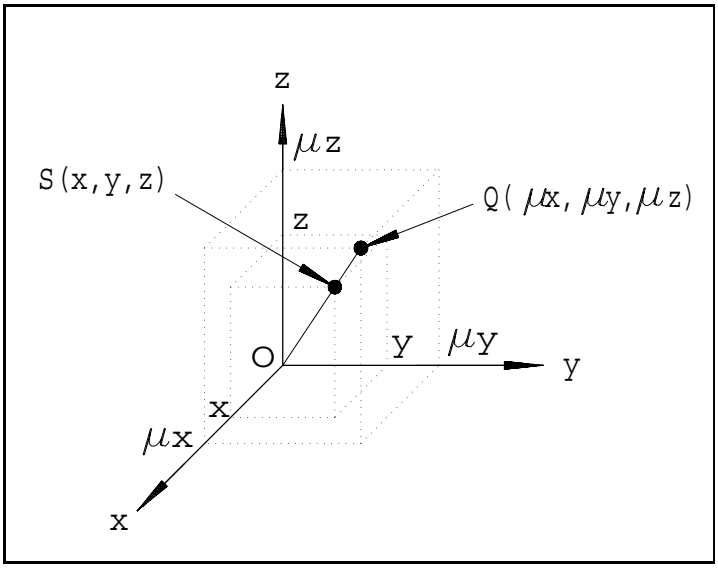

FIGURE 2.2. Cartesian coordinates in E^3.

2.3. A Kinematic Mapping of Planar Displacements

2.3.1. Planar Displacements. A general displacement in the plane requires three independent coordinates to fully characterize it. In other words, a position of one rigid body relative to another is given by three numbers. Typically, a displacement is described by $D(a, b, \phi)$, where a and b are the components of a position vector in the directions of linearly independent basis vectors, and ϕ is a rotation angle about some fixed axis normal to the plane, see Fig. 2.3. In 1911, Grünwald and Blaschke independently suggested using the three numbers which describe a planar position as the coordinates of the points in a three dimensional projective space, called the *image space* [**33, 8**]. This was done originally to gain a deeper insight, and to derive new theorems, of plane kinematics.

A planar motion is a continuous series of displacements, hence a complete motion in the plane is mapped to a curve of the image space. One, two, and three degree of freedom planar motions are represented respectively by curves, surfaces, and solids

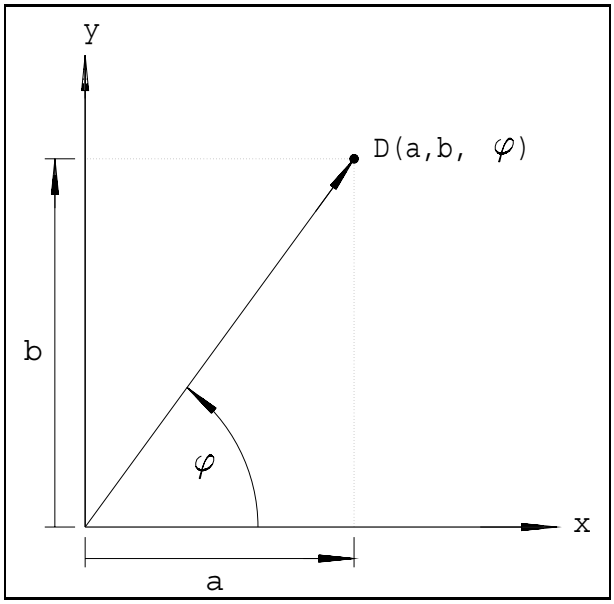

FIGURE 2.3. A planar displacement described by $D(a, b, \phi)$.

in the image space [**39**]. The classification of planar motions can be reduced to the classification of curves, surfaces, and solids [**46**].

It is convenient to think of the relative planar motion between two rigid bodies as the motion of a Cartesian reference coordinate system, E, attached to one of the bodies, with respect to the Cartesian coordinate system, Σ, attached to the other [**8**]. Without loss of generality, Σ may be considered as fixed while E is free to move. Then the position of a point in E relative to Σ can be given by

$$\begin{bmatrix} X' \\ Y' \end{bmatrix} = \begin{bmatrix} \cos\phi & -\sin\phi \\ \sin\phi & \cos\phi \end{bmatrix} \begin{bmatrix} x' \\ y' \end{bmatrix} + \begin{bmatrix} a \\ b \end{bmatrix}, \tag{2.3.1}$$

where

(i) (x', y') are the Cartesian coordinates of a point in E.

(ii) (X', Y') are the Cartesian coordinates of the same point in Σ.

(iii) (a, b) are the Cartesian coordinates of the origin of E measured in Σ, i.e., the components of the position vector of the origin of E in Σ.

(iv) ϕ is the rotation angle measured from the X'–axis to the x'–axis, the positive sense being counter–clockwise.

Equation (2.3.1) does not represent a linear transformation. This fact is computationally inconvenient, and can be remedied by the use of homogeneous coordinates, $(x : y : z)$ and $(X : Y : Z)$, where [**52**]

$$x' = \frac{x}{z} \quad , \quad y' = \frac{y}{z},$$
$$X' = \frac{X}{Z} \quad , \quad Y' = \frac{Y}{Z}.$$

Substituting these homogeneous coordinates in equation (2.3.1) gives for X'

$$\frac{X}{Z} \quad = \quad \frac{x}{z}\cos\phi - \frac{y}{z}\sin\phi + a. \tag{2.3.2}$$

Without loss of generality, the homogenizing coordinates may be set to be equal since their value is arbitrary, i.e. set $Z = z$. Multiplying through by z gives

$$X \quad = \quad x\cos\phi - y\sin\phi + az.$$

Similarly, the Y' expression becomes

$$Y \quad = \quad x\sin\phi + y\cos\phi + bz.$$

The following linear transformation is obtained:

$$\begin{bmatrix} X \\ Y \\ Z \end{bmatrix} \quad = \quad \begin{bmatrix} \cos\phi & -\sin\phi & a \\ \sin\phi & \cos\phi & b \\ 0 & 0 & 1 \end{bmatrix} \begin{bmatrix} x \\ y \\ z \end{bmatrix}, \tag{2.3.3}$$

which may be expressed very compactly as the vector–matrix equation

$$\mathbf{X} = \mathbf{A}\mathbf{x}. \tag{2.3.4}$$

Equation (2.3.4) represents a displacement of E with respect to Σ. If $\mathbf{A}$ is a continuous function of a parameter, such as time, then equation (2.3.4) represents a motion of E with respect to Σ.

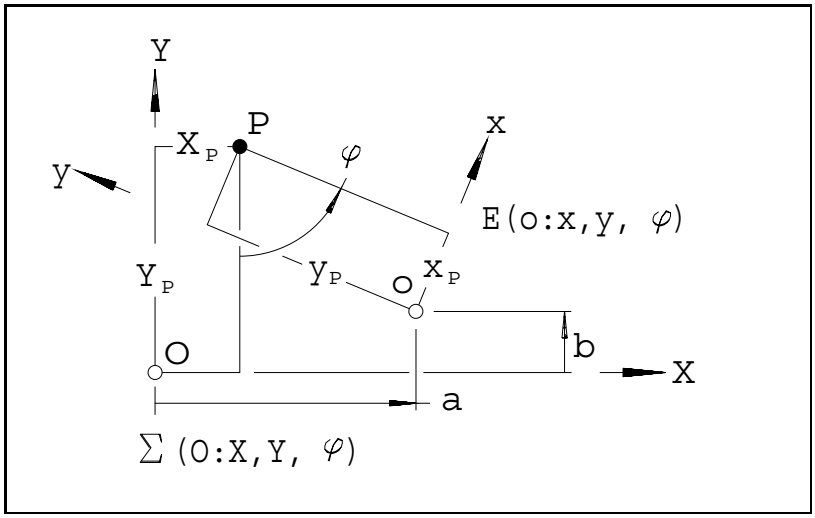

FIGURE 2.4. The pole is an invariant of a planar displacement.

2.3.2. The Pole of a Displacement. All general planar displacements that are not translations may be represented by a single rotation through a finite angle about a fixed axis normal to the plane [**15**]. Even a pure translation can be considered a rotation through an infinitesimal angle about a point at infinity on a line perpendicular to the direction of the translation. The coordinates of the piercing point of this axis describe the *pole* of the displacement. If E and Σ are initially coincident, then after the displacement the pole has the same coordinates in both E and Σ. This is illustrated in Figure 2.4, where P represents the pole and the p–subscripted quantities are the *pole coordinates* in their respective coordinate systems.

To prove that the pole is an invariant of the displacement, the eigenvalues of the 3×3 homogeneous transformation matrix $\mathbf{A}$ are examined [**39**]. The eigenvalue problem is stated as follows:

$$\begin{aligned} \lambda\mathbf{x} &= \mathbf{A}\mathbf{x}, \\ (\mathbf{A} - \lambda\mathbf{I})\mathbf{x} &= \mathbf{0}, \end{aligned}$$

where $\mathbf{x}$ is column vector, λ is a scalar constant, and $\mathbf{I}$ is the 3×3 identity matrix.

The system of equations has non–trivial solutions if, and only if

$$\det\left(\mathbf{A} - \lambda\mathbf{I}\right) \;=\; 0.$$

The 3rd order characteristic polynomial for this 3×3 matrix is found by the Laplacian expansion of the above determinant:

$$\begin{aligned}
(1-\lambda)([\cos\phi - \lambda][\cos\phi - \lambda] + \sin^2\phi) &= 0,\\
(1-\lambda)(\lambda^2 - 2\lambda\cos\phi + \cos^2\phi + \sin^2\phi) &= 0,\\
(1-\lambda)(\lambda^2 - 2\lambda\cos\phi + 1) &= 0.
\end{aligned}$$

Since the characteristic is 3rd order, there must be three eigenvalues. By inspection, the first eigenvalue is $\lambda_1 = 1$. The second and third are from

$$\begin{aligned}
\lambda_{2,3} &= \frac{1}{2}(2\cos\phi \pm \sqrt{4\cos^2\phi - 4}),\\
&= \cos\phi \pm \sqrt{\cos^2\phi - 1},\\
&= \cos\phi \pm \sqrt{-\sin^2\phi},\\
&= \cos\phi \pm \sin\phi\sqrt{-1},\\
&= \cos\phi \pm i\sin\phi,\\
&= e^{\pm i\phi}.
\end{aligned}$$

Hence, for any general planar displacement the homogeneous transformation matrix has only one real eigenvalue, $\lambda = 1$. Corresponding to this eigenvalue, the eigenvalue–matrix equation is quite similar to equation (2.3.4)

$$\mathbf{x} \;=\; \mathbf{A}\mathbf{x}.$$

Now, re–consider equation (2.3.4). It can be *de–homogenized* and expressed as

$$\begin{bmatrix} X' \\ Y' \end{bmatrix} \;=\; \begin{bmatrix} \cos\phi & -\sin\phi \\ \sin\phi & \cos\phi \end{bmatrix} \begin{bmatrix} x' \\ y' \end{bmatrix} + \begin{bmatrix} a \\ b \end{bmatrix}. \tag{2.3.5}$$

If it is true that the pole is an invariant, then its coordinates must be the same in E and in Σ, i.e., $X'_p = x'_p$ and $Y'_p = y'_p$. Substituting these into the previous equation

gives

$$\begin{bmatrix} x'_p \\ y'_p \end{bmatrix} = \begin{bmatrix} \cos\phi & -\sin\phi \\ \sin\phi & \cos\phi \end{bmatrix} \begin{bmatrix} x'_p \\ y'_p \end{bmatrix} + \begin{bmatrix} a \\ b \end{bmatrix}. \tag{2.3.6}$$

This is compactly expressed as

$$\mathbf{x'}_p = \mathbf{B}\mathbf{x'}_p + \mathbf{d}, \tag{2.3.7}$$

where the components of the vector $\mathbf{x'_p}$ are x_p and y_p, $\mathbf{B}$ is the 2×2 rotation matrix and $\mathbf{d}$ is the translation vector whose components are a and b.

It is a simple matter to solve for $\mathbf{x'}_p$:

$$\begin{aligned} \mathbf{x'}_p - \mathbf{B}\mathbf{x'}_p &= \mathbf{d}, \\ (\mathbf{I} - \mathbf{B})\mathbf{x'}_p &= \mathbf{d}, \\ \mathbf{x'}_p &= (\mathbf{I} - \mathbf{B})^{-1}\mathbf{d}. \end{aligned}$$

The last equation may be rearranged as

$$\mathbf{x'}_p = -(\mathbf{B} - \mathbf{I})^{-1}\mathbf{d}. \tag{2.3.8}$$

These are the Cartesian coordinates of the pole.

Return now to the eigenvalue problem,

$$(\mathbf{A} - \lambda\mathbf{I})\mathbf{x} = \mathbf{0}.$$

Setting $\lambda = 1$, the only real eigenvalue for the matrix $\mathbf{A}$,

$$(\mathbf{A} - \mathbf{I})\mathbf{x} = \mathbf{0}.$$

The matrix $(\mathbf{A} - \mathbf{I})$ can be partitioned as

$$\begin{bmatrix} (\mathbf{B} - \mathbf{I}) & \mathbf{d} \\ \mathbf{0}_{1\times 3} & 0 \end{bmatrix} \mathbf{x} = \mathbf{0}. \tag{2.3.9}$$

Equation (2.3.9) may be de–homogenized and expanded giving

$$(\mathbf{B} - \mathbf{I})\mathbf{x'} + \mathbf{d} = \mathbf{0}.$$

Solving for the eigenvector, $\mathbf{x'}$ yields

$$\mathbf{x'} = -(\mathbf{B} - \mathbf{I})^{-1}\mathbf{d}. \tag{2.3.10}$$

Comparing equations (2.3.8) and (2.3.10) it is seen that the eigenvector which corresponds to the sole real eigenvalue shared by all planar homogeneous displacement transformation matrices is identical to the pole of the displacement. Since it is an eigenvector, the pole is coordinate system independent, and hence, invariant.

2.3.3. Pole Coordinates in Terms of a, b and ϕ. Given that the pole P is defined as the point where $X_P = x_P$ and $Y_P = y_P$, as in Fig. 2.4, one may immediately write $a = a(x_P, y_P, \phi)$ and $b = b(x_P, y_P, \phi)$ as

$$\begin{aligned} a &= x_P + y_P \sin\phi - x_P \cos\phi, \\ b &= y_P - y_P \cos\phi - x_P \sin\phi. \end{aligned}$$

Solving for x_P and y_P yields

$$x_P = \frac{a}{2} - \frac{b \sin\phi}{2(1 - \cos\phi)}$$

and

$$y_P = \frac{a \sin\phi}{2(1 - \cos\phi)} + \frac{b}{2}.$$

The homogenizing coordinate is z and its value may now, without loss of generality, be set to $z = \sin\frac{\phi}{2}$. x_P and y_P must also be multiplied by this value. Then the double angle relationships

$$\sin 2\theta = 2\sin\theta\cos\theta, \quad \cos 2\theta = \cos^2\theta - \sin^2\theta$$

are used to obtain the following:

$$\begin{aligned} X_p = \quad x_p = \quad & \frac{1}{2}a\sin(\phi/2) - \frac{1}{2}b\cos(\phi/2), \\ Y_p = \quad y_p = \quad & \frac{1}{2}a\cos(\phi/2) + \frac{1}{2}b\sin(\phi/2), \\ Z_p = \quad z_p = \quad & \sin\phi/2. \end{aligned} \tag{2.3.11}$$

Hence, the homogeneous coordinates of the pole, which are identical in each of the two coordinate systems Σ and E, in terms of the three displacement parameters a, b, and ϕ are determined by the three equations (2.3.11).

2.3.4. The Image Point and Image Space. The location of the pole of a displacement along with the rotation angle convey sufficient information to characterize the displacement. The image of the pole under the kinematic mapping is called the *image point*. Many mappings can be defined that map a position (a, b, ϕ) of the moving coordinate system E with respect to the fixed system Σ in the plane to a point described by the homogeneous coordinates $(X_1 : X_2 : X_3 : X_4)$ of a three dimensional projective *image space*, Σ'. The mapping used here is

$$(X_1 : X_2 : X_3 : X_4) \;=\; (X_p : Y_p : Z_p : \tau Z_p), \tag{2.3.12}$$

where

$$\begin{aligned} (X_1 : X_2 : X_3 : X_4) &\neq (0 : 0 : 0 : 0), \\ \tau &= \cot(\phi/2), \\ 0 \leq \phi &< 2\pi, \end{aligned}$$

and $X_p : Y_p : Z_p$ depend on (a, b, ϕ) as given by the set of equations 2.3.11. The image point is given by

$$\begin{aligned} (X_1 : X_2 : X_3 : X_4) = [&(a\sin(\phi/2) - b\cos(\phi/2) : \\ &(a\cos(\phi/2) + b\sin(\phi/2) : \\ &2\sin(\phi/2) : 2\cos(\phi/2)]. \end{aligned} \tag{2.3.13}$$

By virtue of the relationships expressed in (2.3.13), the linear transformation operator, the matrix $\mathbf{A}$ from equation (2.3.4), may be expressed in terms of the homogeneous coordinates of the image space, Σ'. Recall that

$$\mathbf{A} \;=\; \begin{bmatrix} \cos\phi & -\sin\phi & a \\ \sin\phi & \cos\phi & b \\ 0 & 0 & 1 \end{bmatrix}.$$

A_{11} and A_{22} may be re–expressed using the identities $\cos^2(\phi/2) = (1+\cos\phi)/2$ and $\sin^2(\phi/2) = (1-\cos\phi)/2$. This gives

$$\begin{aligned} X_4^2 - X_3^2 &= (2\cos(\phi/2))^2 - (2\sin(\phi/2))^2, \\ &= \frac{4+\cos\phi)}{4} - \frac{4-\cos\phi)}{4}, \\ &= 4\cos\phi. \end{aligned} \tag{2.3.14}$$

A_{12} and A_{21} are related by $A_{12} = -A_{21}$. A_{12} may be obtained from

$$2X_3X_4 = 2\left[(2\sin(\phi/2))(2\cos(\phi/2))\right]. \tag{2.3.15}$$

The identity

$$2\sin(\phi/2) = \frac{\sin\phi}{\cos(\phi/2)}$$

is used to get

$$2\left[\frac{\sin\phi}{\cos(\phi/2)}2\cos(\phi/2)\right] = 4\sin\phi. \tag{2.3.16}$$

A_{13} is obtained from

$$\begin{aligned} 2(X_1X_3 + X_2X_4) &= 2[(a\sin(\phi/2) - b\cos(\phi/2))(2\sin(\phi/2)) \\ &\quad +(a\cos(\phi/2) + b\sin(\phi/2))(2\cos(\phi/2))], \\ &= 4(a\sin^2(\phi/2) - b\cos(\phi/2)\sin(\phi/2)) + \\ &\quad 4(a\cos^2(\phi/2) + b\cos(\phi/2)\sin(\phi/2)), \\ &= 4a. \end{aligned} \tag{2.3.17}$$

A_{23} is obtained from

$$\begin{aligned} 2(X_2X_3 - X_1X_4) &= 2[(a\cos(\phi/2) + b\sin(\phi/2))(2\sin(\phi/2)) \\ &\quad -(a\sin(\phi/2) - b\cos(\phi/2))(2\cos(\phi/2))], \\ &= 4(a\cos(\phi/2)\sin(\phi/2) + b\sin^2(\phi/2)) - \\ &\quad 4(a\cos(\phi/2)\sin(\phi/2) - b\cos^2(\phi/2)), \\ &= 4b. \end{aligned} \tag{2.3.18}$$

A_{33} is obtained from

$$\begin{aligned} X_3^2 + X_4^2 &= (2\sin(\phi/2))^2 + (2\cos(\phi/2))^2, \\ &= 4. \end{aligned} \tag{2.3.19}$$

Notice that 4 is a factor common to all non zero terms of $\mathbf{A}$. Since homogeneous coordinates are used,

$$\mathbf{X} = \mathbf{A}\mathbf{x} = 4\mathbf{A}\mathbf{x}.$$

So, equation (2.3.3) may be re–expressed using the homogeneous coordinates of the image space. This means that we now have a linear transformation, or a kinematic mapping, to express a position of E with respect to Σ in terms of the image point as given by (2.3.13):

$$\begin{bmatrix} X \\ Y \\ Z \end{bmatrix} = \begin{bmatrix} (X_4^2 - X_3^2) & -2X_3X_4 & 2(X_1X_3 + X_2X_4) \\ 2X_3X_4 & (X_4^2 - X_3^2) & 2(X_2X_3 - X_1X_4) \\ 0 & 0 & (X_4^2 + X_3^2) \end{bmatrix} \begin{bmatrix} x \\ y \\ z \end{bmatrix}. \tag{2.3.20}$$

It may now be said that for each unique displacement described by (a, b, ϕ) there is a corresponding unique point in the image space, because equation (2.3.20) is a linear transformation. From equation (2.3.13), the inverse mapping is obtained. That is, for a given point of the image space, the displacement parameters, or *pre–image* are

obtained from

$$\begin{aligned} \tan(\phi/2) &= X_3/X_4, \\ a &= 2(X_1X_3 + X_2X_4)/(X_3^2 + X_4^2), \\ b &= 2(X_2X_3 - X_1X_4)/(X_3^2 + X_4^2). \end{aligned} \tag{2.3.21}$$

The geometry of the image space is discussed in detail in appendix A.

2.4. Displacements With One Point Bound to a Circle

2.4.1. Planar SG Type Platforms. A planar SG type platform is a manipulator that consists of a movable platform connected to a base by three legs of variable length. Each leg is either an R–P–R or a 3R leg. Figure 2.5 shows the 3R variety. The lengths, r_j, $j \in \{A, B, C\}$ between the platform connection points, A, B, C and corresponding base points, A_0, B_0, C_0 is varied directly with the prismatic pair in the R–P–R type, or by changing the relative angle, ϑ_j, $j \in \{A, B, C\}$ between the two links in the 3R leg. If the r_j are fixed the platform points must be on corresponding circles centred at A_0, B_0, and C_0 with radii r_j.

A moving reference frame E, which moves with the triangular platform, has its origin incident on the platform point A. A non–moving reference frame Σ, with origin incident on the point A_0, is fixed to the base of leg A. Each leg consists of a 2R grounded leg connected to the triangular platform by another R–pair. What remains when legs B and C are disconnected from the platform is a single 2R open chain. Since r_A is fixed in magnitude, the two leg links behave as a single rigid body. They can only rotate about the point A_0. The platform can rotate about A. It is clear that all allowable displacements of this 3R chain require that the point A remain bound to the circle centred at A_0 with radius r_A. Thus, two parameters are required to describe a displacement of the moving frame E with respect to Σ, the fixed frame.

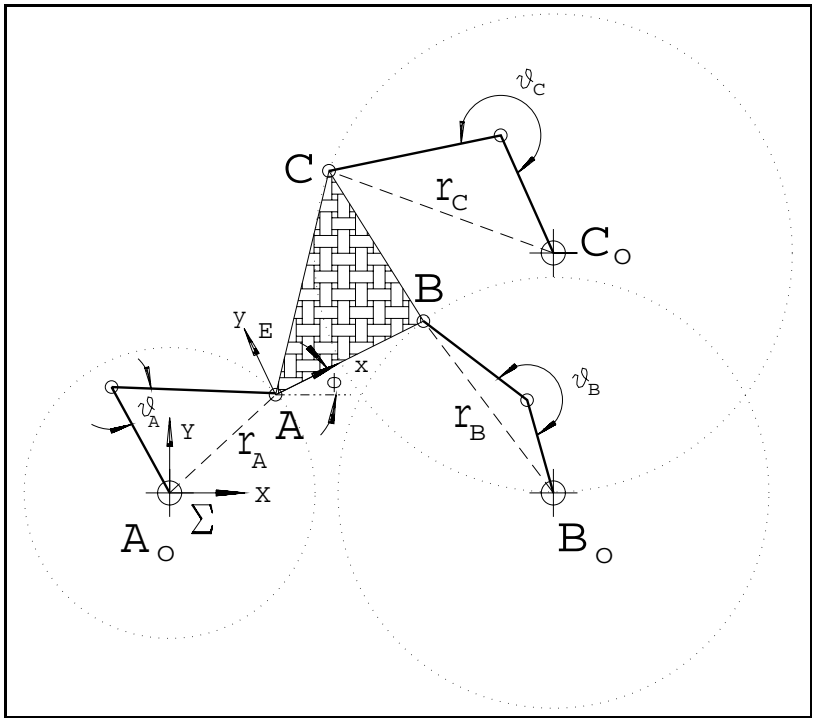

FIGURE 2.5. A planar SG type platform with three 3R legs.

For a given set of input angles, ϑ_j, the platform points must be on circles of radii r_j. Thus, the locations of the platform on the respective circles are the FK solutions.

Husty [**34**] showed that kinematic mapping is a good tool for solving the FK problem for SG type platforms because of the condition that one point of the moving system is bound to a circle. This gives a quadratic condition for the corresponding image points of the possible positions of the platform. Moreover, the mapping does not depend on the platform geometry.

2.4.2. The Hyperboloidal Constraint Manifold. The image of the possible displacements has to be a two parameter set of points, which is a surface in the image space. Bottema and Roth [**8**] show that it is a quadric surface, specifically a hyperboloid. The points on this hyperboloid correspond to all possible positions of the $2R$ open sub–chain, hence all image points are constrained to lie on this surface. McCarthy [**39**] points out that these constraint hyperboloids are manifolds. Husty

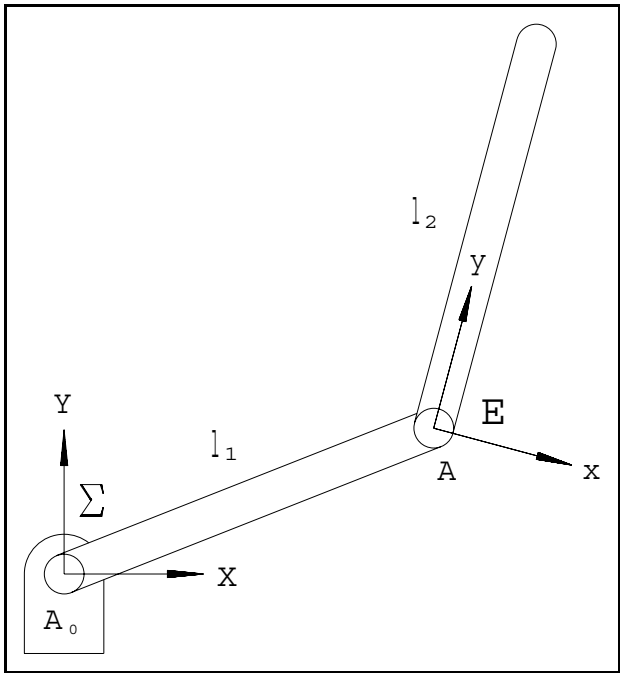

FIGURE 2.6. A planar 2R serial kinematic chain.

[**35**] demonstrates that the constraint manifolds are skew hyperboloids, not necessarily hyperboloids of revolution. Furthermore, Husty shows the intersection curve of the hyperboloid with planes $X_3 = constant$ are circles, and that the axis of the hyperboloid is independent of link length.

Consider the 2R serial chain in Fig. 2.6. Σ and E are arbitrary fixed and moving coordinate reference frames, respectively. Without loss of generality, Σ is fixed to the grounded base with its origin incident on A_0, and E is attached to link l_2, with its origin at the point A. The point A is constrained to move on a circle of radius l_1. Furthermore, link l_2 is free to rotate about point A. The positions of this two parameter system map to a hyperboloid in the image space. Each possible assembly mode of the 2R chain corresponds to a point on the hyperboloid. Since all positions are constrained to be on this quadric, it is called the constraint hyperboloid, H.

The equation of this quadric, H (which is derived in Section 5.2) is found using equation (2.3.20) and the fact that the moving point A is bound to a circle with

radius r, and centre described by the homogeneous coordinates $(X_c : Y_c : Z)$ with respect to the fixed reference frame Σ. The standard hyperboloid equation is

$$\begin{aligned} H: \quad 0 = {} & z^2(X_1^2 + X_2^2) + (1/4)[(x^2 + y^2) - 2C_1xz - 2C_2yz + C_3z^2]X_3^2 + \\ & (1/4)[(x^2 + y^2) + 2C_1xz + 2C_2yz + C_3z^2]X_4^2 + (C_1z - x)zX_1X_3 + \\ & (C_2z - y)zX_2X_3 - (y + C_2z)zX_1X_4 + (C_1z + x)zX_2X_4 + \\ & (C_2x - C_1y)zX_3X_4, \end{aligned} \tag{2.4.1}$$

where

$$\begin{aligned} C_1 &= -X_c, \\ C_2 &= -Y_c, \\ C_3 &= X_c^2 + Y_c^2 - r^2. \end{aligned}$$

For example, suppose $C_1 = C_2 = 0$ and $C_3 = -16$. Furthermore, let the homogenizing coordinates have the values $z = X_4 = 1$. With these simplifications, the equation of the constraint surface H is reduced to

$$H: \quad 0 = X_1^2 + X_2^2 - 4X_3^2 - 4. \tag{2.4.2}$$

This surface is clearly a hyperboloid of one sheet in the variables X_1, X_2, X_3, see Fig. 2.7.

The essential idea of Husty's FK solution algorithm [**33, 34**] is to determine the constraint surfaces for each 2R sub–chain. The assembly modes are the positions which are common to all three constraint surfaces, i.e., the intersections of the hyperboloids. The algorithm is discussed in greater detail in Section 5.2.

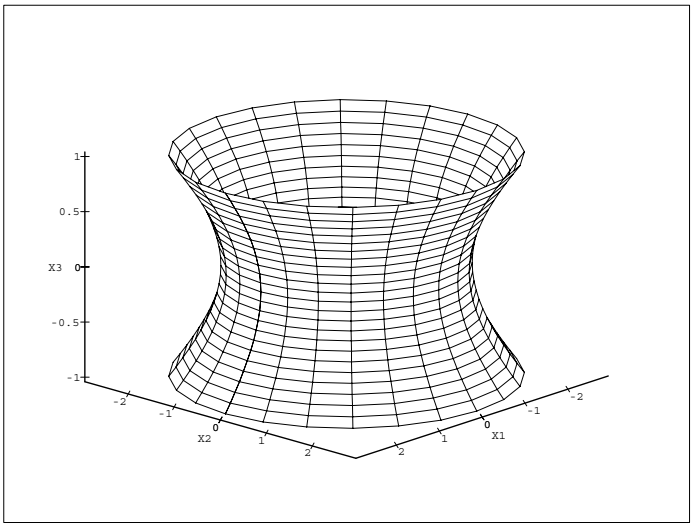

FIGURE 2.7. The constraint hyperboloid, H in the image space.

2.5. Gröbner Bases

Determining the intersections of the three hyberboloids requires the solution of a system of three non–linear equations in three unknowns. Common tools for solving such systems are the *iterative* (Newton–Raphson, etc.), *continuation*, and *elimination* methods [**44, 45**]. However, one thing shared by these methods is that they ignore the geometric properties of the solution space and do not take possible alternate descriptions of the system into account [**1**].

Gröbner bases were introduced in the Ph.D. thesis of Bruno Buchberger, written in 1965 at the University of Innsbruck, Austria. They were named in honour of Wolfgang Gröbner, Buchberger's research supervisor. The essential idea is a generalisation of the theory of univariate polynomials and finite systems of linear equations to multivariate and non–linear systems. The *Buchberger algorithm* [**1, 6**], which computes Gröbner bases, is an extension of the *division algorithm* for polynomial long division, the method of determining *least common multiples* (lcm) of certain terms of two polynomials, and the *Euclidean algorithm* for determining the greatest common divisor

(gcd) of two polynomials. Thus, given a finite set of multivariate polynomials over a field, the Buchberger algorithm computes a new set of polynomials, called Gröbner bases, which are generators of the same ideal as the original.

The *minimal Gröbner basis* of a given ideal can be thought of as basis vectors. That is, every polynomial in the ideal is generated by a linear combination of the minimal Gröbner basis. The *variety*, or solution space, of the Gröbner basis is identical to the variety of the ideal. It is important to note that a variety is determined by an ideal, not by a particular set of equations, or polynomials. Depending on the given ideal, it may be that the set of equations which comprise the Gröbner basis are 'easier' to solve than the given set of the ideal.

The advantage of using Gröbner bases theory over numerical methods, such as the Newton-Raphson or secant methods, is that the reduction is algebraic, not numeric. The potential advantage over the continuation and elimination methods is that the reduced system may require less effort to solve. The biggest potential drawback is that for difficult problems intermediate results can become very large, which usually leads to excessive computational time [**44, 45**].

A very detailed description of Gröbner bases theory may be found in [**1**] and [**6**]. Most of the notation from [**1**] will be used here so that additional information will be easily accessible from that reference.

2.6. Term Orders

Systems of linear equations can be transformed using Gauss–Jordan elimination to the reduced row echelon form. This is the form of the coefficient matrix where every row has a leading '1' with zeros directly beneath and above it. This system has the same solutions as the original but, in general, requires less computational effort to solve. Gröbner bases theory offers an analogous procedure for non–linear

systems. This method involves finding a 'better' representation for the corresponding variety (solution space), meaning that the original non–linear system is now 'easier' to solve. The desired 'better' representation for the variety $V(f_1, \ldots, f_s)$ will be a 'better' generating set for the ideal $I = \langle f_1, \ldots, f_s \rangle$. 'Better', in this case, means the new set of generators give a better understanding of the algebraic structure of $I = \langle f_1, \ldots, f_s \rangle$, and the geometric structure of $V(f_1, \ldots, f_s)$.

Buchberger's algorithm for computing Gröbner bases is essentially a generalisation of the Euclidean algorithm for determining the gcd of two univariate polynomials. It may also be viewed as Gauss-Jordan row reduction for systems of non–linear equations. Employing Gauss-Jordan elimination or the Euclidean algorithm requires a certain ordering of terms. For example, univariate polynomials are ordered by term degree, with the leading term having the highest degree if the division or Euclidean algorithms are to be used. For solving linear systems, the order is unimportant, but it must be specified. For multivariate systems, an analogous order is required.

Recall that the set of power products is denoted by

$$B^n \quad = \quad \{x_1^{\beta_1}, \ldots, x_n^{\beta_n} | \beta_i \in N, i = 1, \ldots, n\}.$$

Let $\boldsymbol{x}^{\boldsymbol{\beta}} = x_1^{\beta_1}, \ldots, x_n^{\beta_n}$, where $\boldsymbol{\beta} = (\beta_1, \ldots, \beta_n) \in N^n$. It will be assumed that the different terms in a polynomial have different power products, so $3x^2y$ would never be written as $2x^2y + x^2y$. The terms in a polynomial are arranged in increasing or decreasing order, hence there must be a way to compare any two power products. The order must be a *total order*. That is, given any $\boldsymbol{x}^{\boldsymbol{\alpha}}, \boldsymbol{x}^{\boldsymbol{\beta}} \in B^n$, exactly one of the following must be true:

$$\boldsymbol{x}^{\boldsymbol{\alpha}} < \boldsymbol{x}^{\boldsymbol{\beta}}, \quad \boldsymbol{x}^{\boldsymbol{\alpha}} = \boldsymbol{x}^{\boldsymbol{\beta}}, \quad \text{or } \boldsymbol{x}^{\boldsymbol{\alpha}} > \boldsymbol{x}^{\boldsymbol{\beta}}.$$

The following three total term orders are used effectively in determining Gröbner bases [**1, 6**].

DEFINITION 2.6.1. *Let* lex *denote the* lexicographical *order on* B^n *with* $x_1 > x_2 > \ldots > x_n$ *and be defined as follows: If*

$$\boldsymbol{\alpha} = (\alpha_1, \ldots, \alpha_n), \boldsymbol{\beta} = (\beta_1, \ldots, \beta_n) \in N^n$$

then

$$\boldsymbol{x^\alpha} < \boldsymbol{x^\beta} \iff \begin{cases} \textit{the first coordinates } \alpha_i \textit{ and } \beta_i \textit{ in } \boldsymbol{\alpha} \textit{ and } \boldsymbol{\beta} \\ \textit{from the left which are different satisfy } \alpha_i < \beta_i. \\ \textit{“From the left” means starting with the largest variables.} \end{cases}$$

For example, in the commutative polynomial ring $k[x, y]$ with lex $x < y$, the following order is implied

$$1 < x < x^2 < x^3 < \ldots < y < xy < x^2y < \ldots < y^2 < \ldots .$$

DEFINITION 2.6.2. *Let* deglex *denote the* degree lexicographical *order on* B^n *with* $x_1 > x_2 > \ldots > x_n$ *and be defined as follows: If*

$$\boldsymbol{\alpha} = (\alpha_1, \ldots, \alpha_n), \boldsymbol{\beta} = (\beta_1, \ldots, \beta_n) \in N^n$$

then

$$\boldsymbol{x^\alpha} < \boldsymbol{x^\beta} \iff \begin{cases} \sum_{i=1}^n \boldsymbol{\alpha_i} < \sum_{i=1}^n \boldsymbol{\beta_i} \\ \textit{or} \\ \sum_{i=1}^n \boldsymbol{\alpha_i} = \sum_{i=1}^n \boldsymbol{\beta_i} \textit{ and } \boldsymbol{x^\alpha} < \boldsymbol{x^\beta} \\ \textit{with respect to } \text{lex} \textit{ with } x_1 > \ldots > x_n \end{cases}$$

In the commutative polynomial ring $k[x, y]$ the degree lexicographical ordering deglex with $x < y$ is

$$1 < x < y < x^2 < xy < y^2 < x^3 < x^2y < xy^2 < y^3 < \ldots$$

The final term ordering is the *degree reverse lexicographical* order.

DEFINITION 2.6.3. *Let* degrevlex *denote the* degree reverse lexicographical *order on* B^n *with* $x_1 > x_2 > \ldots > x_n$ *and be defined as follows: If*

$$\boldsymbol{\alpha} = (\alpha_1, \ldots, \alpha_n), \boldsymbol{\beta} = (\beta_1, \ldots, \beta_n) \in N^n$$

then

$$\boldsymbol{x^{\alpha}} < \boldsymbol{x^{\beta}} \iff \begin{cases} \sum_{i=1}^{n} \boldsymbol{\alpha_i} < \sum_{i=1}^{n} \boldsymbol{\beta_i} \\ \textit{or} \\ \sum_{i=1}^{n} \boldsymbol{\alpha_i} = \sum_{i=1}^{n} \boldsymbol{\beta_i} \textit{ and the first coordinates } \alpha_i \textit{ and } \beta_i \textit{ in} \\ \boldsymbol{\alpha} \textit{ and } \boldsymbol{\beta} \textit{ from the right, which are different, satisfy } \alpha_i > \beta_i. \end{cases}$$

In this case, "from the right" means that the smallest variables are compared until a set of corresponding exponents are found that have different values.

In the case of two variables, deglex and degrevlex are identical. But, if there are three or more variables in the ring this is no longer the case. This can be seen in the following example:

$$x_1^2 x_2 x_3 > x_1 x_2^3 \quad \text{for deglex with} \quad x_1 > x_2 > x_3$$

but, if the degrevlex order is used the opposite is true:

$$x_1^2 x_2 x_3 < x_1^2 x_2^3 \quad \text{for degrevlex with} \quad x_1 > x_2 > x_3.$$

Using degrevlex the exponents of x_3 are compared because they are the first from the right that are different. That is, on the left hand side the exponent of x_3 is 1, on the right hand side is exponent is 0. The tie is broken because $1 > 0$, hence $\boldsymbol{x^{\alpha}} < \boldsymbol{x^{\beta}}$.

To compare the three term orderings, consider the polynomial in $k[x, y, z]$, described by $f = 4x^2y^2z - 10xy^4 + 2x^4$.

$$\begin{aligned} \text{lex with } x > y > z &\implies xy^4 < x^2y^2z < x^4, \\ &\implies f = 2x^4 + 4x^2y^2z - 10xy^4. \end{aligned}$$

$$\begin{aligned} \text{deglex with } x > y > z &\implies x^4 < xy^4 < x^2y^2z, \\ &\implies f = 4x^2y^2z - 10xy^4 + 2x^4. \end{aligned}$$

$$\begin{aligned} \text{degrevlex with } x > y > z &\implies x^4 < x^2y^2z < xy^4, \\ &\implies f = -10xy^4 + 4x^2y^2z + 2x^4. \end{aligned}$$

Again, note that for the degrevlex ordering, to break the tie the first set of different exponents from the right are those of z. Since $1 > 0$ then $x^2y^2z < xy^4$.

2.7. The Univariate Case

2.7.1. The Euclidean Algorithm. The algorithm attributed to Euclid is for determining the gcd of two positive integers. Suppose a and b are positive integers with $a > b$. Then for some integers q_1 and r_1, $0 \leq r_1 < b$,

$$a = q_1 b + r_1.$$

Since $r_1 < b$, we also have

$$b = q_2 r_1 + r_2,$$

where q_2 and r_2 are integers, with $0 \leq r_2 < r_1$.

Successive divisions produce the sequence of equations

$$\begin{array}{ll} a = q_1 b + r_1, & 0 \leq r_1 < b \\ b = r_1 q_2 + r_2, & 0 \leq r_2 < r_1 \\ r_1 = r_2 q_3 + r_3, & 0 \leq r_3 < r_2 \\ \vdots & \vdots \\ r_{n-2} = r_{n-1} q_n + r_n, & 0 = r_n < r_{n-1} < r_{n-2}. \end{array}$$

Since the successive remainders are decreasing non–negative integers, the remainder $r_n = 0$ must be obtained after a finite number of divisions. The gcd of a and b is the last positive remainder in the sequence. This is so because r_{n-1} is a divisor of each divisor and of each remainder. It must, therefore, be a divisor of each dividend, and the gcd of a and b is the same as that of r_{n-2} and r_{n-1}, namely, r_{n-1} [**18**].

The operations used in the Euclidean algorithm are addition and division. These operators may also be used on polynomials. Hence, the Euclidean algorithm may be used to determine the gcd of two polynomials. The main tool in the Euclidean algorithm is the division algorithm.

2.7.2. The Univariate Polynomial Division Algorithm. The *degree* of a polynomial f, denoted by $\deg(f)$, is the largest exponent of x in f. The *leading term* of f, $\mathrm{lt}(f)$, is the highest degree term of f. The *leading coefficient* of f, $\mathrm{lc}(f)$, is the

TABLE 2.1. Polynomial term reference terminology.

Symbol	Meaning
$\deg(f)$	Degree of polynomial f
$\mathrm{lt}(f)$	The leading term of polynomial f
$\mathrm{lc}(f)$	The leading coefficient of polynomial f
$\mathrm{lp}(f)$	The leading power product of polynomial f

coefficient of $\mathrm{lt}(f)$. The *leading power product* of f, $\mathrm{lp}(f)$, is the power product of the leading term, $\mathrm{lt}(f)$. These are summarised in Table 2.1.

The polynomial f is divisible by the polynomial g if and only if $\deg(g) \leq \deg(f)$. Consider the two polynomials

$$\begin{aligned} f &= a_n x^n + a_{n-1} x^{n-1} + \ldots + a_1 x + a_0 \\ g &= b_m x^m + b_{m-1} x^{m-1} + \ldots + b_1 x + b_0, \end{aligned}$$

with $n = \deg(f) \geq m = \deg(g)$. If this is so, then g *divides* f.

The first step in the division of f by g is to subtract from f the product $\frac{a_n}{b_m} x_{n-m} g$. The factor of g in this product is $\dfrac{\mathrm{lt}(f)}{\mathrm{lt}(g)}$. The remainder after the first division step is denoted by r_1 and is given by

$$r_1 = f - \frac{\mathrm{lt}(f)}{\mathrm{lt}(g)} g.$$

r_1 is called a *reduction* of f by g and the process of computing r_1 is indicated by

$$f^g \longrightarrow r_1.$$

$\deg(r_1)$ is necessarily less than $\deg(f)$ due to the subtraction of a suitable multiple of g, which eliminates $\mathrm{lt}(f)$. If $\deg(r_1) > \deg(g)$ the process continues, reducing r_1 by g to obtain r_2 as

$$r_2 = r_1 - \frac{\mathrm{lt}(r_1)}{\mathrm{lt}(g)} g.$$

The division algorithm continues until the final remainder equals zero, or the degree of the remainder is less than $\deg(g)$. At this point $\mathrm{lt}(g)$ can no longer be used to

eliminate lt(r). If the polynomial division required three steps to obtain the final remainder, the reduction could be represented by

$$f^g \longrightarrow r_1^g \longrightarrow r_2^g \longrightarrow r.$$

However, the following shorthand may be used to indicate that repeated reduction steps were used.

$$f^g \longrightarrow_+ r.$$

Note that an ordering of the polynomials is implied. That is, for the algorithm to terminate, the final remainder r must be zero, or have a degree less than that of g. This can only occur if the powers of x are ordered with $x^m < x^n$ and $m < n$. The last condition, $m < n$ is equivalent to the statement that x^m divides x^n [**1**].

It is well established [**24, 18, 11**] that, given a non–zero polynomial $g \in k[x]$, for any $f \in k[x]$ with deg(k) $\geq$deg(g), $\exists$ q, the quotient, and the remainder, r, both $\in k[x]$ such that

$$f \;\; = \;\; qg + r, \text{with } r = 0 \text{ or } \deg(r) < \deg(g).$$

Moreover, q and r are unique.

Next, consider an ideal $I = \langle f_1, f_2 \rangle \in k[x]$. The gcd of f_1 and f_2 will have a variety identical to $V(f_1, f_2)$ [**1**]. Hence, it may be that the system $(f_1, \ldots, f_s)$ can be solved with less computational effort if $g = \gcd(f_1, \ldots, f_s)$ is first computed with the Euclidean algorithm. Then all solutions to the system are obtained by solving $g = 0$. Furthermore, any other polynomial in $k[x]$ for which the remainder is zero upon division by g is in I. g is said to *generate* I, and is the 'best' generator for the ideal.

2.8. The Multivariate Case

2.8.1. Multivariate Polynomial Division Algorithm. Now, consider the case of ideals generated by more than two multivariate polynomials, $I = \langle f_1, \ldots, f_s \rangle$. In order to divide f by $f_1, \ldots, f_s$ requires a reworking of the division and Euclidean algorithms given earlier. The general idea is the same as for linear and univariate polynomials: cancel terms of f using the leading terms of the f_i's, so that new terms are smaller order than the cancelled terms, and continue the process of subtracting multiples of the f_i's until the remainder has a smaller degree than any of the f_i's. One complicating factor is that the dividend may have more than one divisor.

Given $f, g, h \in k[x_1, \ldots, x_n]$ with $g \neq 0$, the reduction symbol given earlier

$$f^g \longrightarrow h$$

may be thought of as f reducing to h modulo g, if and only if $\mathrm{lp}(g)$ divides a non–zero term $\boldsymbol{x}^{\boldsymbol{\alpha}}$ that appears in f, and

$$h \;=\; f - \frac{\boldsymbol{x}^{\boldsymbol{\alpha}}}{\mathrm{lt}(g)} g.$$

In this regard, h is the remainder of a one step division of f by g. This process of subtracting off terms in f that are divisible by $\mathrm{lt}(g)$ continues until $h = 0$, or $\deg(h) > \deg(g)$. This final remainder is denoted by r.

Let f, h, and $f_1, \ldots, f_s$ be polynomials in $k[x_1, \ldots, x_n]$, with $f_i \neq 0 (1 \leq i \leq s)$, and let $F = \{f_1, \ldots, f_s\}$. Then

$$f^F \longrightarrow_+ h$$

is the notation for f reduces to h modulo F, if and only if there exists a sequence of indices $i_1, i_2, \ldots, i_t \in \{1, \ldots, s\}$ and a sequence of polynomials $h_1, \ldots, h_{t-1} \in k[x_1, \ldots, x_n]$ such that

$$f^{f_{i_1}} \longrightarrow h_1^{f_{i_2}} \longrightarrow h_2^{f_{i_3}} \longrightarrow \ldots^{f_{i_{t-1}}} \longrightarrow h_{t-1}^{f_{i_t}} \longrightarrow h.$$

If $h = 0$ or there is no power product in h that is divisible by any of the $\mathrm{lp}(f_i)$, then h is *reduced* with respect to the set of non–zero polynomials F. Such a reduced polynomial is a *remainder* and is called r. In other words, r can not be reduced modulo F. This reduction process allows for the definition of a multivariate division algorithm, analogous to the univariate case. Given $f, f_1, \ldots, f_s \in k[x_1, \ldots, x_n]$ with $f_i \neq 0$, the algorithm below returns quotients $u_i, \ldots, u_s \in k[x_1, \ldots, x_n]$, and a remainder $r \in k[x_1, \ldots, x_n]$, such that

$$f = u_1 f_1 + \ldots + u_s f_s + r.$$

Note that in this algorithm an ordering is assumed among the polynomials in the set $\{f_1, \ldots, f_s\}$ when i is chosen to be least such that $\mathrm{lp}(f_i)$ divides $\mathrm{lp}(h)$.

ALGORITHM 2.8.1. Multivariate Polynomial Division Algorithm.

INPUT: $f, f_1 \ldots, f_s \in k[x_1, \ldots, x_n]$ with $f_i \neq 0 (1 \leq i \leq s)$
OUTPUT: $u_1, \ldots, u_s, r$ such that $f = u_1 f_1 + \ldots + u_s f_s + r$ and
r is reduced with respect to $\{f_1, \ldots, f_s\}$ and
$\max(\mathrm{lp}(u_1)\mathrm{lp}(f_1), \ldots, \mathrm{lp}(u_s)\mathrm{lp}(f_s), \mathrm{lp}(r)) = \mathrm{lp}(f)$.
INITIALIZATION: $u_1 := 0, \ldots, u_s := 0, r := 0, h := f$
WHILE $h \neq 0$ **DO**
IF $\exists\ i$ such that $\mathrm{lp}(f_i)$ divides $\mathrm{lp}(h)$ **THEN**
choose the least i such that $\mathrm{lp}(f_i)$ divides $\mathrm{lp}(h)$

$$\begin{aligned} u_i &:= u_i + \frac{\mathrm{lt}(h)}{\mathrm{lt}(f_i)} \\ h &:= h - \frac{\mathrm{lt}(h)}{\mathrm{lt}(f_i)} f_i \end{aligned}$$

ELSE

$$\begin{aligned} r &:= r + \mathrm{lt}(h) \\ h &:= h - \mathrm{lt}(h) \end{aligned}$$

CONTINUE

END

2.8.2. Definition of Gröbner Bases.

DEFINITION 2.8.1. *A* Gröbner Basis *for an ideal I is a set of non–zero polynomials $G = \{g_1, \ldots, g_t\}$ contained in I if and only if for all $f \in I$ such that $f \neq 0$, $\exists$ $i \in \{1, \ldots, t\}$ such that lp(g_i) divides lp(f).*

If G is a Gröbner basis for I, then all polynomials in I can be reduced with respect to G. For a subset S of $k[x_1, \ldots x_n]$, the *leading term ideal of* S is defined to be the ideal

$$\mathrm{Lt}(S) \;=\; \langle \mathrm{lt}(s) | s \in S \rangle.$$

With this definition in mind, the following statements are equivalent [**1**]:

(i) G is a Gröbner basis for I.

(ii) $f \in I$ if and only if $f^G \longrightarrow_+ 0$.

(iii) Lt(G) =Lt(I).

The proof for the existence of G is given in [**1**].

2.8.3. *S*–Polynomials and Buchberger's Theorem.

DEFINITION 2.8.2. *Let $0 \neq f, g \in k[x_1, \ldots, x_n]$. Let the* least common multiple (lcm) *of two power products be denoted L =lcm(lp(f),lp(g)). The polynomial*

$$S(f,g) \;=\; \frac{L}{\mathrm{lt}(f)} f - \frac{L}{\mathrm{lt}(g)} g$$

is defined to be the S–polynomial *of f and g.*

S–polynomials are used for the following reason. In the division of f by $f_1, \ldots, f_s$, it may happen that some term $\boldsymbol{x^\alpha}$ in f is divisible by both lp(f_i) and lp(f_j) with $i \neq j$, hence, $\boldsymbol{x^\alpha}$ is divisible by L =lcm(lp(f_i),lp(f_j)). If f is reduced by f_i then

$$h_1 \;=\; f - \frac{\boldsymbol{x^\alpha}}{f_i} f_i$$

is obtained. On the other hand, if f is reduced by f_j

$$h_2 \;=\; f - \frac{\boldsymbol{x}^{\boldsymbol{\alpha}}}{f_j} f_j$$

will be obtained. The ambiguity introduced is

$$h_2 - h_1 = \frac{\boldsymbol{x}^{\boldsymbol{\alpha}}}{f_i} f_i - \frac{\boldsymbol{x}^{\boldsymbol{\alpha}}}{f_j} f_j = \frac{\boldsymbol{x}^{\boldsymbol{\alpha}}}{L} S(f_i, f_j).$$

A key theorem concerning S–polynomials is due to Buchberger.

THEOREM 2.8.1. (Buchberger) *Let $G = \{g_1, \ldots, g_t\}$ be a set of non–zero polynomials in $k[x_1, \ldots, x_n]$. G is a Gröbner basis for the ideal $I = \langle g_1, \ldots, g_t \rangle$ if and only if for all $i \neq j$,*

$$S(g_i, g_j)^G \longrightarrow_+ 0.$$

Buchberger's proof is given in [**1**].

2.8.4. Buchberger's Algorithm. The Buchberger theorem outlines a strategy for computing Gröbner bases: Reduce the S–polynomials and if a remainder is non–zero, add it to the list of polynomials in the generating set. Continue doing this until there are 'enough' polynomials in the generating set to make all S–polynomials reduce to zero. Buchberger's algorithm will produce a Gröbner basis for the ideal $I = \langle f_1, \ldots, f_s \rangle$, given $F = \{f_1, \ldots, f_s\}$ with $f_i \neq 0 (1 \leq i \leq s)$.

ALGORITHM 2.8.2. Buchberger's Algorithm for Computing Gröbner bases.
INPUT: $F = \{f_1, \ldots, f_s\} \subseteq k[x_1, \ldots, x_n]$ with $f_i \neq 0 (1 \leq i \leq s)$

OUTPUT: $G = \{g_1, \ldots, g_s\}$, a Gröbner basis for I

INITIALIZATION: $G := F, \mathcal{G} := \{\{f_i, f_j\} | f_i \neq f_j \in G\}$

WHILE $\mathcal{G} \neq 0$ **DO**

Choose any $\{f, g\} \in \mathcal{G}$

$\mathcal{G} := \mathcal{G} - \{\{f, g\}\}$

$S(f, g)^G \longrightarrow_+ h$, where h is reduced with respect to G

IF $h \neq 0$ **THEN**

$\mathcal{G} \cup \{\{u, h\} | \ \forall \ u \in G\}$

$G := G \cup \{h\}$

CONTINUE

END

2.8.5. Minimal Gröbner Bases. It can be shown [**1**] that there exists a set of minimal Gröbner bases for every ideal. This leads to the important definition:

DEFINITION 2.8.3. *A Gröbner basis* $G = \{g_1, \ldots, g_t\}$ *is called* minimal *if for all* i, $\mathrm{lc}(g_i)$*=1 and for all* $i \neq j$, $\mathrm{lp}(g_i)$ *does not divide* $\mathrm{lp}(g_j)$.

2.9. Example

EXAMPLE 2.9.1.

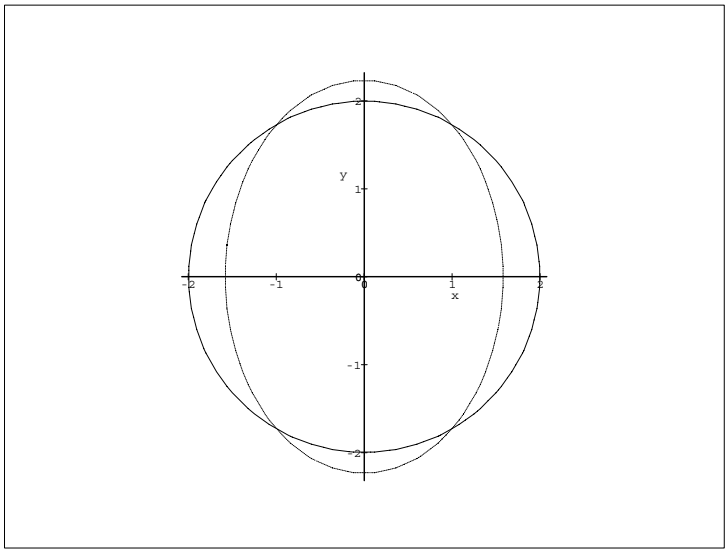

FIGURE 2.8. Non–linear equations f_1 & f_2: Intersecting circle and ellipse.

Consider a set of non–linear equations in two variables. Let the first equation represent a circle with radius 2, given by $x^2 + y^2 = 4$. It is required to determine the

variety of the set, i.e., the set of real intersections (if any) of this circle with the ellipse described by $2x^2 + y^2 = 5$. These two equations may be rearranged as polynomials in two variables, x and y:

$$f_1 : \quad x^2 + y^2 - 4, \tag{2.9.1}$$

$$f_2 : \quad 2x^2 + y^2 - 5. \tag{2.9.2}$$

A plot of these geometric entities reveals that they do, indeed, have four intersections. This is shown in Fig. 2.8. Hence, the variety is not the empty set.

The goal of this example is to illustrate how the Buchberger algorithm computes a Gröbner basis for the ideal I. First, a term ordering is required. We will choose lex with $y < x$, specify the input to the algorithm, and proceed:

INITIALIZATION: $G := \{f_1, f_2\}, \mathcal{G} := \{\{f_1, f_2\}\}$

Pass one through the WHILE loop:

$\mathcal{G} := \{\{f_1, f_2\}\} - \{\{f_1, f_2\}\} = 0$

$$\begin{aligned} S(f_1, f_2) &= \frac{L}{\mathrm{lt}(f_1)} f_1 - \frac{L}{\mathrm{lt}(f_2)} f_2 \\ &= \frac{x^2}{x^2}(x^2 + y^2 - 4) - \frac{x^2}{2x^2}(2x^2 + y^2 - 5) \\ &= \frac{1}{2}y^2 - \frac{3}{2} \end{aligned}$$

$S(f_1, f_2) = \frac{1}{2}y^2 - \frac{3}{2}$ can be reduced by neither f_1 or f_2.
Then $S(f_1, f_2)^G \longrightarrow_+ h \neq 0$.
This being the case, let $f_3 := \frac{1}{2}y^2 - \frac{3}{2}$.
Continuing with the first pass:

$\mathcal{G} := \{\{f_1, f_3\}\{f_2, f_3\}\}$
$G := \{f_1, f_2, f_3\}$

Pass two through the WHILE loop:

Choose $\{\{f_1, f_3\}\} \in \mathcal{G}$
$\mathcal{G} := \{\{f_2, f_3\}\}$

$$\begin{aligned} S(f_1, f_3) &= \frac{x^2y^2}{x^2}(x^2+y^2-4) - \frac{x^2y^2}{(y^2/2)}(\frac{1}{2}y^2 - \frac{3}{2}) \\ &= 3x^2 + y^4 - 4y^2 \\ &= 3f_1 + (2y^2-8)f_3 + 0. \end{aligned}$$

This implies that

$S(f_1, f_3)^G \longrightarrow_+ 0 = h$

Pass three through the While loop:

Choose $\{\{f_2, f_3\}\} \in \mathcal{G}$

$\mathcal{G} := 0$

$$\begin{aligned} S(f_2, f_3) &= \frac{x^2y^2}{2x^2}(2x^2+y^2-5) - \frac{x^2y^2}{(y^2/2)}(\frac{1}{2}y^2 - \frac{3}{2}) \\ &= 3x^2 + \frac{1}{2}y^4 - \frac{5}{2}y^2 \\ &= 3f_1 + (y^2-8)f_3 + 0. \end{aligned}$$

This implies that

$S(f_2, f_3)^G \longrightarrow_+ 0 = h$

The WHILE loop stops, since $\mathcal{G} = 0$.

$G := \{f_1, f_2, f_3\}$

Hence, a set of Gröbner basis consists of the original second degree polynomials plus a third univariate second degree polynomial. However, this is not a problem because the minimal Gröbner basis can always be determined. It is readily shown that $\mathrm{lp}(f_2)$ and $\mathrm{lp}(f_1)$ divide each other. f_4 can be obtained as a linear combination of f_1 and f_2.

$$\begin{aligned} f_4 &= f_2 - f_1, \\ &= 2x^2 + y^2 - 5 - (x^2 + y^2 - 4), \\ &= x^2 - 1. \end{aligned}$$

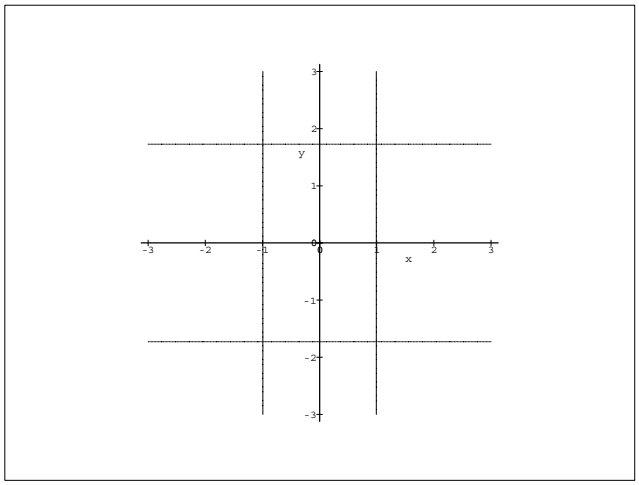

FIGURE 2.9. The set of four orthogonal lines.

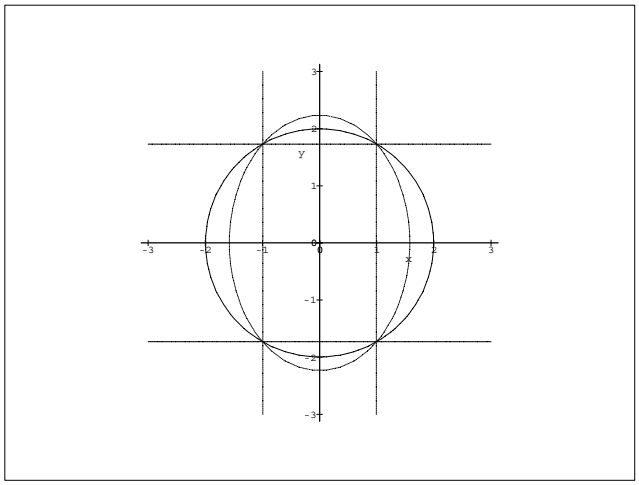

FIGURE 2.10. The variety $V(f_1, f_2)$ is identical to $V(f_4, f_5)$.

Finally, multiply f_3 through by 2 to get $f_5 = 2f_3 = y^2 - 3$. This gives the minimal Gröbner basis for $I = \langle f_1, f_2 \rangle$:

$$G \;=\; \{x^2 - 1, y^2 - 3\}. \tag{2.9.3}$$

Every polynomial in the ideal to which f_1 and f_2 belong can be expressed as a linear combination of the minimal Gröbner basis, f_4 and f_5. Geometrically, f_4 and f_5 represent a set of two pairs of orthogonal lines, shown in Fig. 2.9. Clearly then, the points shared by the lines $x = \pm\sqrt{1}$ and $y = \pm\sqrt{3}$ are the same as those shared by $x^2 + y^2 = 4$ and $2x^2 + y^2 = 5$. The variety $V(f_1, f_2)$ is identical to the variety $V(f_4, f_5)$, as can be seen in Fig. 2.10. The difference is that the system $\{f_4, f_5\}$ requires less computational effort to solve than $\{f_1, f_2\}$.

Chapter 3

Manipulator Description

3.1. Holonomic Planar Rolling System

3.1.1. Manipulator Description. A manipulator with 3 closed kinematic chains, or loops (A_0B_0, A_0C_0, B_0C_0), is shown in Fig. 3.1. It consists of 7 articulated rigid elements, which move with constrained relative motion, and a rigid grounded base. These 8 members are connected by 6 R–pairs and 3 G–pairs. The end–effector, disk D, is the link -G-G- in each -R-R-G-G-R-R- loop. Legs A, B, and C each consist of two links.

Fig. 3.2 shows the disk and a single leg. The first link in each leg is grounded to the base, connected by an R–pair and to the second link by another R–pair. The circular disk rolls, without slip, along the straight lines Q^jS^j (in general, $j \in \{A, B, C\}$ throughout this text) on the non–grounded links of each of three 2R serial legs. Although these lines remain in tangential contact with the disk, the points of tangency can be varied by relative rolling between the lines and disk.

3.1.2. Holonomic Higher Pairs. Referring to Fig. 3.1, the points of contact, P_C^j, between the disk and legs constitute three *holonomic* higher kinematic pairs. The term refers to the fact that the constraint equations are in integral form, that is, in terms of displacement. The constraint equation is simply the arc length equation for a circular arc. It may be expressed in terms of the displacement of the points of contact along lines Q^jS^j and the appropriate IAC. Furthermore, the pure rolling

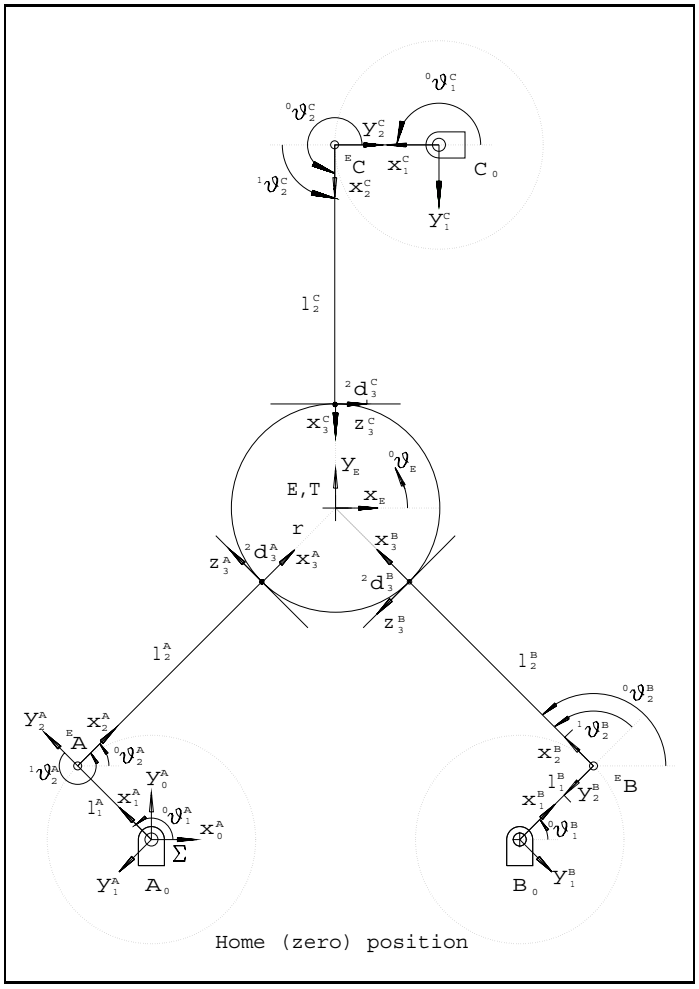

FIGURE 3.1. A planar manipulator with three holonomic higher pairs.

condition and that fact that the displacements are planar allows the simple, linear arc length equation to express the constraint for the higher pairs. Because of these related conditions, the higher pairs are holonomic.

3.2. Nomenclature

The IK analysis of a parallel manipulator is the same as that for a serial manipulator, except that the solution is repeated for each leg [**20**]. Moreover, the kinematic mapping procedure for the FK analysis also considers each leg separately [**33, 34**].

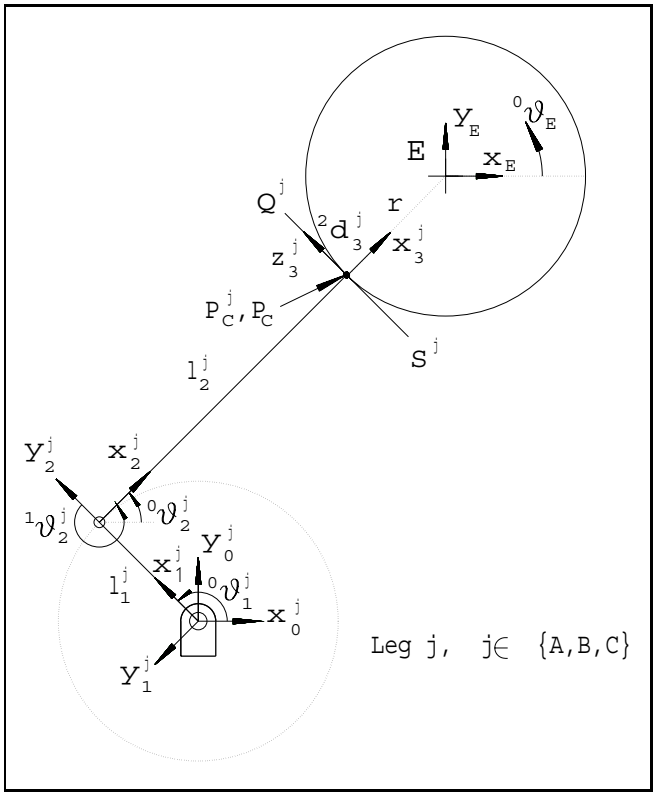

FIGURE 3.2. One of the three 2R legs and the disk.

Hence, joint and position variables along with link design parameters must be described so as to allow for analysis of the manipulator on a leg by leg basis. To minimise the confusion that results from the handling of the kinematic relationships in component form, a system of left and right sub and super–scripts shall be adopted. Each joint and position variable is fully identified by left and right sub and super–scripts while link parameters require only right sub and super–scripts. The system described below is intended for use with the IK algorithm. Certain modifications are required for the FK procedure and are detailed in section 3.2.6. Referring to Fig. 3.2, consider the generic parameter

$$ {}^{f}_{m}\psi^{j}_{i}. $$

3.2.1. Left and right sub and super–scripts.

(i) For a joint variable, the right sub–script i, $i \in \{1, 2, 3\}$ identifies the joint number. For each manipulator leg, the joint number at the connection between the first link and the base is 1. Between the first and second link is 2. The higher pair between link 2 and the disk is 3.

(ii) For a coordinate axis, the right sub–script i, $i \in \{0, 1, 2, 3\}$ represents the link to which the coordinate system is attached. 0 is for the base, 1 is for the first link, etc..

(iii) The right super–script, j, $j \in \{A, B, C\}$ denotes a particular manipulator leg.

(iv) The left super–script, f, $f \in \{0, 1, 2, 3\}$ refers to the reference frame in which the variable is represented.

(v) The left sub–script, m indicates the type of planar motion. R is for pure rotation of the disk about its centroid. T is for pure translation of the disk centre. No left sub–script means either general plane motion, or that the type of motion is obvious from the context.

3.2.2. Fixed link design parameters.

(i) l_i^j is the length of link i in leg j and r is the radius of the disk.

(ii) l_{0x}^{jk} is the projected distance along the horizontal axis of the inertial reference frame, $\{{}_0^A\}$ between the origins of legs j and k, $j \in \{A, B, C\}$, $k \in \{A, B, C\}$.

Note 1: For all analysis in this thesis the non–moving reference frame, $\{{}_0^A\}$, attached to the base of leg A is considered as the inertial reference frame. In Chapter 5 it is referred to as Σ.

Note 2: If $j = k$, the value of this parameter, as well as the one below, is zero since there is no base offset distance in this case.

(iii) l_{0y}^{jk} is the projected distance along the vertical axis of the inertial reference frame, $\{{}_0^A\}$ between the origins of legs j and k, $j \in \{A, B, C\}$, $k \in \{A, B, C\}$.

3.2.3. Joint variables.

(i) ${}^{f}_{m}\vartheta^{j}_{i}$ is the joint angle i of leg j described in reference frame f with regard to m type of motion. Positive angles are measured counter–clockwise (CCW).

(ii) ${}^{2}_{m}d^{j}_{3}$ is the distance from point P^j to point P^j_C measured along y^j_2. Note that y^j_2 and z^j_3 are always parallel. So d^j_3 could be measured in frame $\{{}^{j}_{3}\}$ along z^j_3. However, in order to later derive the manipulator displacement equations using Denavit and Hartenberg (DH) parameters [**17**], d^j_3 must be expressed in frame $\{{}^{j}_{2}\}$. In the home position shown in Fig. 3.2, the points P^j and P^j_C are coincident. The origin of the frame $\{\ {}^{j}_{3}\ \}$ is superimposed on the point of contact between the straight line Q^jS^j, and the disk D, and translates with it along line Q^jS^j.

3.2.4. Position variables: The Pose Array. The *pose* of the disk will be described by a 3×1 array. The variables are all expressed in the inertial reference frame, so the left super–script '0', while always implied, is omitted. The array is written as:

$$\begin{bmatrix} x_E \\ y_E \\ \vartheta_E \end{bmatrix},$$

where

x_E is the x Cartesian coordinate of the disk centre,

y_E is the y Cartesian coordinate of the disk centre,

ϑ_E is the orientation of the disk expressed as the angle between the x_E axis and the x^A_0 axis. In the home position, the x_E axis is parallel to the x^A_0 axis.

Because of the pure rolling constraint, the initial pose of the disk must be considered in both the FK and IK problems. The variables corresponding to the home, or

zero position of the manipulator will be scripted with an additional '0'. For example, the pose array in the home position is given by

$$\begin{bmatrix} x_{E0} \\ y_{E0} \\ \vartheta_{E0} \end{bmatrix}.$$

3.2.5. Link Reference Frames. The algebra involved in both the IK and FK problems can be simplified by expressing each joint variable in its own reference frame. Variables in the cascaded reference frames are transformed to other reference frames as the problem requires. Careful selection of frame origins further simplifies computation. Hence, link reference frames (with the exception of frames E and T) are assigned using the well established procedure developed by Denavit and Hartenberg [**17, 26**] and adapted here for higher pairs. The procedure is summarised below [**16**]:

(i) Identify the point of intersection, or the common normal of neighbouring joint axes i and $i+1$. Assign the origin of the frame for link i at the point of intersection, or where the common normal meets the i^{th} axis.

(ii) Assign the z_i direction pointing along the i^{th} joint axis.

(iii) Assign the x_i direction pointing along the common normal, or if the axes intersect, assign x_i to be normal to the plane containing the two axes.

(iv) Assign the y_i direction to complete a right–handed coordinate system.

This procedure introduces the planar systems (x, y) and (x, z), see Figs. 3.1 & 3.2. These systems are used for their computational convenience when concatenating the 4×4 DH parameter transformations (section 4.2) to derive the displacement equations.

3.2.6. Additional Nomenclature for the FK Problem. Additional nomenclature is required to suit the demands of the FK problem. In order to make the transform between actual and *pseudo inputs* (introduced in section 5.1.2) it is convenient to have two reference frames, E and T, attached to the disk. Both E and T

translate with the disk, but only E rotates with the disk. The origins of E and T are both incident on the centre of the disk.

The R–pairs connecting two links in a leg shall be referred to as *knee joints* A, B, and C. Recall that ${}^2d_3^j$, $j \in \{A, B, C\}$ is the distance of the contact point measured along the y_2^j coordinate axis, which is always parallel to the rack. Observe that the Euclidean distance between the knee joint and the centre of the disk is a function of this distance. Also, the three normals through each contact point are all incident on the disk centre. The change in the angle a normal makes with respect to the non–rotating frame, T, is related to the change in position of the contact point along the rack by

$$\Delta^2 d_3^j \;\; = \;\; r\Delta^T \theta_E^j.$$

3.3. Mobility Analysis

An unconstrained rigid body in the plane has three DOF. It can translate in two mutually orthogonal directions in the plane and it can rotate about any axis perpendicular to the plane. This is a special case of general 3 DOF motions in 3–space, where the 3 freedoms can be any of the $\binom{6}{3}$, i.e., 20 permutations of translations and rotations.

l unconstrained rigid links have $3(l-1)$ relative degrees of freedom, given that one of the rigid links is designated as a non–moving reference link. Any joint connecting two neighbouring bodies removes at least one or at most two relative DOF. If the joint removes no DOF then the bodies are not connected. If the joint removes three DOF then the two bodies are a rigid structure.

The general mobility formula for planar motion, often referred to as the Chebyshev–Grübler–Kutzbach formula [**2, 30**], is expressed as:

$$3(l-1) - \sum_{i=1}^{j} u_i \;\; = \;\; \text{DOF}, \tag{3.3.1}$$

where l is the number of links, u_i is the number of constraints imposed by the i_{th} joint, and j is the number of joints.

The three legged manipulator shown in Fig. 3.1 is characterised as follows: Including the base, there are eight links; six R–pairs take away two freedoms each; the three G–pairs also take away two freedoms each. Using the Chebyshev–Grübler–Kutzbach formula:

$$3(8-1) - 6(2) - 3(2) \;\; = \;\; 3. \tag{3.3.2}$$

Since there are 3 DOF, three independent coordinates are required to specify the pose of the disk.

It is worthwhile to note that the disk has 3 DOF regardless of the number of grounded 2R legs to which it is connected by pure rolling. This is proven by showing the left hand side (LHS) of equation (3.3.1) is always equal to 3. Equation 3.3.1 may be re–expressed as:

$$3(l-1) - 2j = \text{DOF}, \tag{3.3.3}$$

since each joint removes two DOF. The ground link and disk always count as two links and each of the n legs is composed of two links, thus for n legs the number of links is

$$l = 2n + 2. \tag{3.3.4}$$

Furthermore each leg has three joints, so:

$$j = 3n. \tag{3.3.5}$$

Substituting equations (3.3.4) and (3.3.5) into the LHS of equation (3.3.3) gives

$$\begin{aligned} & 3(2n+2-1) - 2(3n) \\ = \; & 6n + 3 - 6n \\ = \; & 3. \end{aligned}$$

Therefore, n can be any positive non–zero integer. This implies the disk may have any position and orientation, within the physical limits of its workspace. These 3 DOF are independent of the number of 2R legs upon which the disk rolls.

3.4. Tangency Condition

By virtue of the pure rolling constraints, the straight lines along which the disk rolls must always remain tangent to the disk. Consider a line and a circle in the Euclidean plane. The equation of the line can be represented by the linear equation

$$ax + by + c = 0, \tag{3.4.1}$$

for constant coefficients a, b, c, and variable points (x, y). A circle with centre (x_c, y_c) and radius r is given by

$$(x - x_c)^2 + (y - y_c)^2 - r^2 = 0. \tag{3.4.2}$$

Equation (3.4.1) can be solved for y to give the familiar slope–intercept form of the line, and the expression is substituted into equation (3.4.2). The result is expanded in powers of x which yields a quadratic:

$$Ax^2 + Bx + C = 0, \tag{3.4.3}$$

where:

$$\begin{aligned} A &= \frac{a^2}{b^2} + 1, \\ B &= 2\left(-x_c + \frac{ac}{b^2} + \frac{ay_c}{b}\right), \\ C &= x_c^2 - r^2 + \left((c/b) + y_c\right)^2. \end{aligned}$$

To satisfy the tangency condition, the discriminant of the quadratic must vanish:

$$\sqrt{B^2 - 4AC} \;\; = \;\; 0.$$

The discriminant itself is a quadratic in terms of the constant a:

$$(x_c^2 - r^2)a^2 + (c + by_c)2x_c a + (b^2 y_c^2 - b^2 r^2 + 2bcy_c + c^2) = 0. \tag{3.4.4}$$

This condition is necessary, but not sufficient to guarantee pure rolling contact. However, all solutions to the FK and IK problems must satisfy this condition. FK and IK algorithms can use this condition as a check on the validity of solutions.

3.5. Commutative Disk Displacements in the Plane

Recall section 2.1.2: The group operator defined on $\mathcal{D}$, $*$, is called "product". $*$ represents successive implementations of given isometries. Now, any displacement of the disk, that is, any product of translations and rotations about arbitrary parallel axes normal to the plane may be decomposed into the product of a single translation of the disk centre and a single rotation through a finite angle of the disk about its centre [**14**]. Furthermore, since it is the centre of rotation which is translated, these specific translations and rotations commute. The latter claim is shown by the following: Let

$$\begin{aligned} \mathcal{T}_d &= \text{Translation through distance } d, \\ \mathcal{S}_\Phi &= \text{Rotation through angle } \Phi \text{ about centre } S. \end{aligned}$$

Consider the arbitrary motion of the disk along some path between an initial position, P_i, and a final position, P_f, shown in Fig. 3.3. $\mathcal{T}_d$ is the translation through distance d of the disk centre from P_i to P_f. Although many paths are associated with the isometry $\mathcal{T}_d$, the distance d is independent of the path between the two points. In fact, d is the sum of the directed translations along *any* path between P_i and P_f.

Along any arbitrary path, the disk orientation can change such that when it arrives at P_f, a reference line painted on the disk has been rotated through an angle Φ. This angle is the sum of all angular displacements of the disk about arbitrary parallel axes (perpendicular to the plane of the disk) encountered along the path. This sum

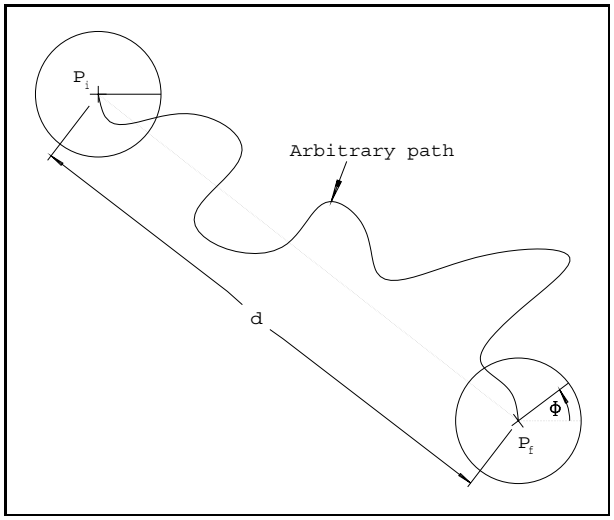

FIGURE 3.3. Arbitrary motion of the disk between two points.

may be expressed as the difference between Φ_f and Φ_i, such that $\Phi_f \equiv \Phi_i(\text{mod}2\pi)$. It follows that the sum of all angular displacements along the path may be expressed as a single rotation of the disk about its centre, $\mathcal{S}_\Phi$, where $\Phi = \Phi_f - \Phi_i$.

Thus, any arbitrary motion of the disk may be represented by the product of a single translation of its centre and a single rotation about its centre. The centre of the disk is a point. Points can not rotate, they can only translate. Since the centre of rotation is translated it is evident that $\mathcal{S}_\Phi$ may occur independently from $\mathcal{T}_d$. It then follows that:

$$\mathcal{T}_d * \mathcal{S}_\Phi \quad = \quad \mathcal{S}_\Phi * \mathcal{T}_d.$$

3.6. Special Geometric Manipulator Properties

The general motion of the disk in the plane involves relative motion between the disk and each serial 2R leg. The rolling contact is conveniently modelled as multiple racks and a single pinion. Each rack can roll on the pinion, the pinion can roll on the racks, or there can be a combination of the two motions. For general planar motion the system, with link frames as assigned in Fig. 3.1, has the following properties:

(i) If the pinion rolls on one rack, then it must roll on all.

(ii) As a consequence of (i), if one of the higher pairs is locked, the disk can not rotate about its centre.

(iii) Any or all of the racks may roll on the pinion.

(iv) If, during general motion, the pinion is stationary with respect to one rack while the other racks roll on the pinion there are two possibilities. Consider leg A, for example. Suppose that the higher pair in this leg is locked. First, if ${}^0\vartheta_2^A$ is constant, the motion of the pinion is pure curvilinear translation in the fixed base frame. Second, if ${}^0\vartheta_2^A$ changes during the motion, then the pinion rotates about a centre other than its own axis by an angle equal to the change in ${}^0\vartheta_2^A$. Regardless, there can be no rotation of the disk about its centre, since one of the higher pairs is locked. Such a motion would violate (ii).

(v) If $\Delta^2 d_3^A$ has the same magnitude but opposite sense as either $\Delta^2 d_3^B$ or $\Delta^2 d_3^C$, then the motion of the pinion is pure rectilinear translation of its centre. Pure curvilinear translation can also occur if the magnitude condition is violated however, the opposite sense condition must be met.

(vi) If $\Delta^2 d_3^A$, $\Delta^2 d_3^B$, and $\Delta^2 d_3^C$ have the same magnitude and sense, then the motion of the pinion is pure fixed axis rotation about its centre.

Chapter 4

The Inverse Kinematics Problem

4.1. Approach

The IK problem involves the determination of a set of feasible joint variables required to attain a desired pose. It may be stated succinctly as: given $[x_E, y_E, \vartheta_E]^T$ determine $[{}^0\vartheta_1^j, {}^1\vartheta_2^j, {}^2d_3^j]^T$. A complicating factor in general plane displacement is the ambiguity that the rolling constraint introduces. That is, ϑ_E, the desired final disk orientation does not divulge how much of the new position was achieved by rotation of the grounded and non–grounded links and how much was achieved by pure rolling between the disk and the legs. By how much has the disk rolled on the racks and by how much has each rack rolled on the disk? Is there a combination, and if so, what is the ratio? These questions lead to difficulties in the calculation of the joint offsets, ${}^2d_3^j$. To address this problem the special properties of the manipulator (section 3.6) and the group properties of $\mathcal{D}$ (section 2.1.2) are invoked. Any feasible displacement of the disk can then be decomposed into a pure translation of the disk and pure, fixed axis rotation about the centre of the disk (see section 3.5).

Given both the desired pose array and the IAC, a set of intermediate joint variables may be calculated for the pure translation component. The translation set may then be combined with a subsequent set calculated for the pure rotation component.

As shown in section 3.5, these rotations and translations commute. Hence, the order of rotation and translation is not important. This last fact will be used for the sake of convention: The intermediate solutions for pure translation will be calculated first. Then, using this intermediate set as new initial conditions, solutions will be generated for fixed axis rotation. The final solution set is simply the combination of the two solution sets.

A result determined in section 4.3.3 is that the upper bound on the number of solutions to the IK problem is 4^n, where n is the number of legs. For the three–legged version, this means that there are as many as 64 real solutions. The aim was to develop an algorithm to determine solutions and not to generate vast tables of data. Since the solutions are not coupled from leg to leg we can, without loss of generality, develop the algorithm using the two–legged version as the model. The solution algorithm can then be applied to similar manipulators with any number of 2R legs. It is for this reason that the two–legged version, shown in Fig. 4.1, is now considered.

4.2. Derivation of Disk Displacement Equations

Input–output displacement equations for each leg are required for the IK algorithm. The inputs for a given leg are the location of the base in the inertial reference frame; the three joint parameters, ${}^0\vartheta_1^j$, ${}^1\vartheta_2^j$, and ${}^2d_3^j$; the IAC. The outputs are the disk position and orientation, x_E, y_E, and ϑ_E. The displacement equations for the two–legged version of the manipulator are readily obtained by inspection. However, the DH notation provides an excellent means for 'accounting' as well as keeping the problem 'general'. After assigning link reference frames by the procedure given in section 3.2.5, the following definitions of link parameters apply [**16, 17**]:

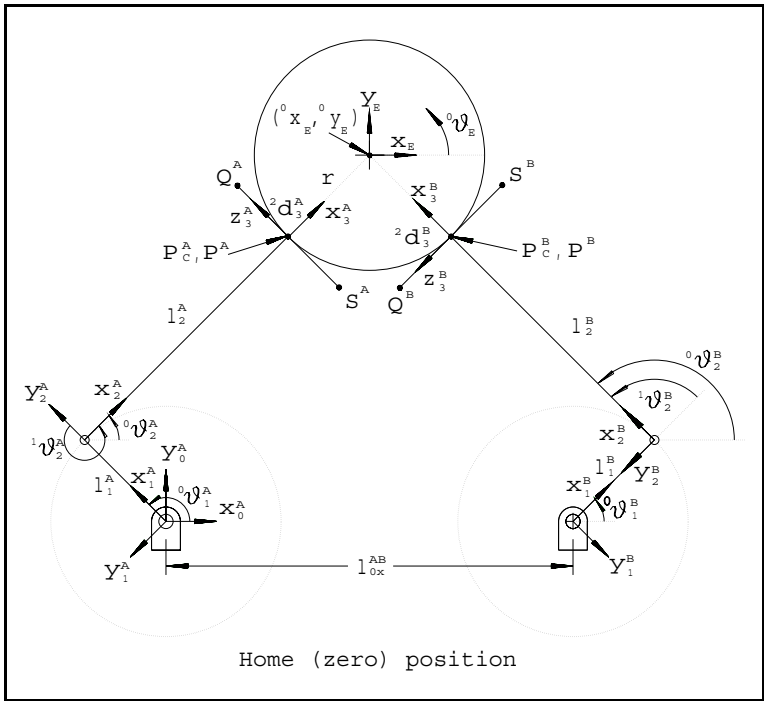

FIGURE 4.1. Disk platform with two 2R legs.

a_i = distance from z_i to z_{i+1} along x_i.
α_i = angle between z_i & z_{i+1} about x_i.
d_i = distance from x_{i-1} to x_i along z_i.
ϑ_i = angle between x_{i-1} & x_i about z_i.

Using homogeneous Cartesian coordinates [**52**] with a homogenising coordinate of $x_h = 1$, the relative displacement between adjacent links can be expressed as a linear transformation of the form:

$$ {}^{i+1}\mathbf{x} \;=\; {}^{i+1}_{i}\mathbf{T}\,{}^{i}\mathbf{x}, $$

where ${}^{i+1}\mathbf{x}$ and ${}^{i}\mathbf{x}$ are the position vectors of points in reference frames $\{i+1\}$ and $\{i\}$ respectively, with $\mathbf{x}$ having the form:

$$ \begin{bmatrix} x \\ y \\ z \\ 1 \end{bmatrix}. $$

Either y or z will be set to zero, depending on which reference plane is used (see Fig. 4.1). The additional dimensions are included for the sake of computation and have

no effect on the outcome. The operator ${}^{i+1}_{i}\mathbf{T}$ is a 4×4 homogeneous transformation matrix which maps vectors defined in frame i into frame $i+1$. Employing the DH parameters, it has the form:

$$ {}^{i+1}_{i}T = \begin{bmatrix} c\vartheta_i & -s\vartheta_i & 0 & a_{i-1} \\ s\vartheta_i c\alpha_{i-1} & c\vartheta_i c\alpha_{i-1} & -s\alpha_{i-1} & -s\alpha_{i-1}d_i \\ s\vartheta_i s\alpha_{i-1} & c\vartheta_i s\alpha_{i-1} & c\alpha_{i-1} & c\alpha_{i-1}d_i \\ 0 & 0 & 0 & 1 \end{bmatrix}, $$

where $c \equiv \cos$ and $s \equiv \sin$.

A transformation matrix must be calculated for each link. The matrices may then be concatenated, in the appropriate order, to obtain the transformation matrix which relates the pose of the disk in the disk frame, $\{E\}$ to the pose of the disk in the base frame of interest. Since the base frame $\{{}^{A}_{0}\}$ has been selected as the inertial reference frame, the locations of the bases of all other legs must be expressed with respect to $\{{}^{A}_{0}\}$ and incorporated into the calculations. The displacement equations for each leg may then be obtained, by inspection, from this transformation matrix.

After some algebra the following equations are obtained (note the right super–script is dropped, since all variables refer to the current leg):

$$ K_x = l_1 c_1 + (l_2 + r)c_{12} - d_3 s_{12}, \tag{4.2.1} $$

$$ K_y = l_1 s_1 + (l_2 + r)s_{12} + d_3 c_{12}, \tag{4.2.2} $$

where

$$ \begin{aligned} K_x &= x_E - l^{Ak}_{0x}, \\ K_y &= y_E - l^{Ak}_{0y}, \\ c_1 &= \cos({}^0\vartheta_1), \\ c_{12} &= \cos({}^0\vartheta_1 + {}^1\vartheta_2), \\ s_1 &= \sin({}^0\vartheta_1), \\ s_{12} &= \sin({}^0\vartheta_1 + {}^1\vartheta_2). \end{aligned} $$

Note that for leg A, $K_x = x_E$, and $K_y = y_E$, because of the location of the origin of the inertial reference frame.

4.3. Inverse Kinematics Algorithm

4.3.1. The Four Algorithm Steps. Since solutions are not coupled between legs, [**20**], each leg is treated as an open four–bar chain and solved for separately. A convention mentioned in section 3.2.2, is that the inertial reference frame will remain coincident with the fixed reference frame on the base of leg A. The choice of leg A is arbitrary, however any subsequent legs will be labelled $B, C, \ldots, j$, CCW from leg A. Leg A will always be solved for first. The inverse kinematics algorithm is summarized, with reference to Fig. 4.1, in the following four steps. Note the dependence of the results on the initial conditions. This dependency is what removes this manipulator from the more common group of SG type planar platforms jointed exclusively with lower pairs.

Step 1. Pure translation: Remove the higher pair connection with all but the leg being considered. The first iteration concerns leg A. Lock the higher pair so that $\Delta^2 d_3^A = 0$ and calculate the joint angles required to reach the new position given by the ordered pair (x_E, y_E). Call the new angles ${}^0_T\vartheta^A_{10}$, ${}^1_T\vartheta^A_{20}$, and ${}^0_T\vartheta^A_{20}$ (recall that ${}^0_T\vartheta^A_{20} = {}^0_T\vartheta^A_{10} + {}^1_T\vartheta^A_{20}$).

Step 2. Remove artificial angular offset: Recall special property (iv) in section 3.6: If the disk is stationary with respect to one rack while in motion, then the disk orientation can change. Since pure translation of the disk is required, any angular offset created by step 1 must be removed. This is accomplished by an imaginary fixed axis rotation about the disk centre equal in magnitude, but opposite in sense to ${}^0_T\vartheta^A_{20}$. Calculate ${}^2_T d_3^A$, which is the joint offset required to effect the imaginary rotation. Recalculate the joint angles. These are the joint angles necessary to cause

the pure translation of the disk centre. Call these intermediate angles ${}^0_T\vartheta_1^A$, ${}^1_T\vartheta_2^A$, and ${}^0_T\vartheta_2^A$. Of course, if there is no rotation component to the motion, these are the final joint angles. If there is no translation component, these angles are the same as the initial joint angles.

Step 3. Pure rotation: Recall special property (vi) in section 3.6: If $\Delta^2 d_3^A$ (ie.,${}^2d_3^A - {}^2d_{30}^A$) and $\Delta^2 d_3^B$ have the same magnitude and sense, then the motion of the disk is pure rotation about its centre. Hence, $\Delta^2 d_3^A$ is simply calculated from the arc length subtended by $\Delta\vartheta_E$ (ie., $\vartheta_E - \vartheta_{E0}$), and is the same for all legs. Using the joint variables from step 2 as initial conditions and the desired disk angle ϑ_E, calculate ${}^0\vartheta_1^A$, ${}^1\vartheta_2^A$, and ${}^2d_3^A$.

Step 4. Repeat Steps 1, 2, and 3 for the remaining legs.

4.3.2. Closed Form Analytic Solution. Once the displacement equations are known, the following procedure may be used to solve for the set of joint variables required to achieve a desired feasible pose. Again, since the solution proceeds on a leg–by–leg basis all variables correspond to the current leg, so the right superscript may be omitted. Equations (4.2.1) and (4.2.2) are squared and added. ${}^0\vartheta_1$ is eliminated using the identities:

$$\begin{aligned} c_{12} &= c_1c_2 - s_1s_2, \\ s_{12} &= c_1s_2 + s_1c_2. \end{aligned}$$

The following equation in two unknowns, ${}^1\vartheta_2$ and ${}^2d_3$, is obtained:

$$\begin{aligned} 0 &= 2l_1((l_2+r)c_2 - {}^2d_3 s_2) + l_2(2r+l_2) + l_1^2 + {}^2d_3^2 \\ &\quad + r^2 - K_x^2 - K_y^2. \end{aligned} \tag{4.3.1}$$

The variable ${}^2d_3$ can be determined because of special property (vi) (in section 3.6) and the fact that the general plane motion is decomposable into pure translational

and rotational components. In the algorithm, step 1 requires that the higher pair be locked. Hence, there is no change in ${}^2d_3$. Step 2 recovers the angular offset artificially caused by step 1. This is accomplished by fixed axis rotation of the disk about its centre. Step 3 is the actual pure rotational component of the motion. Again, this is a fixed axis rotation about the disk centre. Thus ${}^2d_3$ in each of steps 2 and 3 is given by:

$$\text{Step 2:} \quad {}^2_T d_3 = {}^2d_{30} - r({}^0_T\vartheta_{20} - {}^0\vartheta_{20}), \tag{4.3.2}$$

$$\text{Step 3:} \quad {}^2d_3 = {}^2_T d_3 + r(\vartheta_E - \vartheta_{E0}). \tag{4.3.3}$$

Determining the joint offsets using the pure rolling constraint equations guarantees that the tangency condition is met since tangency is a necessary (although not sufficient) condition for pure rolling.

Equation (4.3.1) can now be expressed as a function of just one variable, ${}^1\vartheta_2$:

$$\tan\frac{1}{2}({}^1\vartheta_2) = \left[\frac{K_1 \pm 2\sqrt{K_2}}{2K_3}\right], \tag{4.3.4}$$

where

$$\begin{aligned}
K_1 &= 4l_1{}^2d_3, \\
K_2 &= 2l_1^2(l_2^2 + {}^2d_3^2 + r^2) + 4l_2r(l_1^2 - {}^2d_3^2 + K_x^2 + K_y^2) \\
&\quad -2{}^2d_3^2(l_2^2 + r^2) + 2(K_x^2 + K_y^2)(l_1^2 + l_2^2 + {}^2d_3^2 + r^2) \\
&\quad -2K_x^2K_y^2 - 4l_2^3r - 6r^2l_2^2 - 4r^3l_2 - l_1^4 - l_2^4 \\
&\quad -{}^2d_3^4 - r^4 - K_x^4 - K_y^4, \\
K_3 &= l_1^2 + l_2^2 + {}^2d_3^2 + r^2 - K_x^2 - K_y^2 + 2l_2(r - l_1) \\
&\quad -2l_1r.
\end{aligned}$$

Solving (4.3.4) for ${}^1\vartheta_2$ yields two solutions:

$${}^1\vartheta_2 = 2\tan^{-1}\left[\frac{K_1 \pm 2\sqrt{K_2}}{2K_3}\right]. \tag{4.3.5}$$

Solving for angles using $\tan^{-1}$ has an inherent ambiguity concerning the quadrant in which the angle lies. However, this solution involves the half angle and hence the quadrant is unique.

4.3.3. Upper Bound on the Number of Solutions. For a general displacement, the four algorithm steps produce the following: From step 1 two values of ${}^1_T\vartheta_{20}$ are obtained from equation (4.3.1). Corresponding to each of these there is a unique value of ${}^0_T\vartheta_{10}$ that will satisfy both equations (4.2.1) and (4.2.2). From step 2, there is one value of ${}^2_T d_3$ obtained for each value of ${}^0_T\vartheta_{20}$ determined in step 1. Also, two values of each of ${}^1_T\vartheta_2$ and ${}^0_T\vartheta_1$ are obtained. Step 3 yields two values for ${}^2d_3$, one for each of the values of ${}^2_T d_3$ determined in step 2. For each value of ${}^2d_3$ there correspond two values for each of ${}^1\vartheta_2$ and ${}^0\vartheta_1$. These are the *elbow–up* and *elbow–down* solutions. Thus, for each leg there are up to four solutions. The solutions for each leg are uncoupled. Hence, for a manipulator with n legs, there are 4^n solutions, some of which may be complex conjugate pairs. It must be noted that not all configurations can be achieved by smooth motions from the home position.

4.4. Examples

The following three numerical examples deal with 1) pure rotation of the disk about its centre; 2) pure translation of the disk, no disk rotation; 3) combined translation and rotation. In all three examples, the home position shown in Fig. 4.1 is the initial position. The fixed link parameters and initial conditions are as follows, where lengths are in "generic" units and angles are in degrees:

Initial Pose Array

$$\begin{bmatrix} x_{E0} \\ y_{E0} \\ \vartheta_{E0} \end{bmatrix} = \begin{bmatrix} 5\sqrt{2} \\ 9\sqrt{2} \\ 0^\circ \end{bmatrix}$$

Fixed Link Parameters					
r	$=$	4			
l_{0x}^{AB}	$=$	$10\sqrt{2}$			
l_{0y}^{AB}	$=$	0			
l_1^A	$=$	l_1^B	$=$	4	
l_2^A	$=$	l_2^B	$=$	10	

Initial Joint Parameters				
${}^2d_{30}^A$	$=$	${}^2d_{30}^B$	$=$	0
${}^0\vartheta_{10}^A$	$=$	$135°$		
${}^0\vartheta_{10}^B$	$=$	$45°$		
${}^1\vartheta_{20}^A$	$=$	$270°$		
${}^1\vartheta_{20}^B$	$=$	$90°$		
${}^0\vartheta_{20}^A$	$=$	$45°$		
${}^0\vartheta_{20}^B$	$=$	$135°$		

EXAMPLE 4.4.1.

Pure Rotation: Pure rotation of the disk about its centre is the simplest motion for obtaining solutions. There are no intermediate joint parameters to calculate. As a result, a maximum of only four solutions may be expected.

In this example, the disk centre remains in its home position while it rotates through 15°. The desired pose array is:

$$\begin{bmatrix} x_E \\ y_E \\ \vartheta_E \end{bmatrix} = \begin{bmatrix} 5\sqrt{2} \\ 9\sqrt{2} \\ 15° \end{bmatrix}.$$

The four solutions are given in Table 4.1 at the end of the chapter and are represented graphically in Fig. 4.2.

EXAMPLE 4.4.2.

Pure Translation: In this example, joint parameters are calculated for the case of pure translation of the disk. Despite the fact that no real rotation of the disk

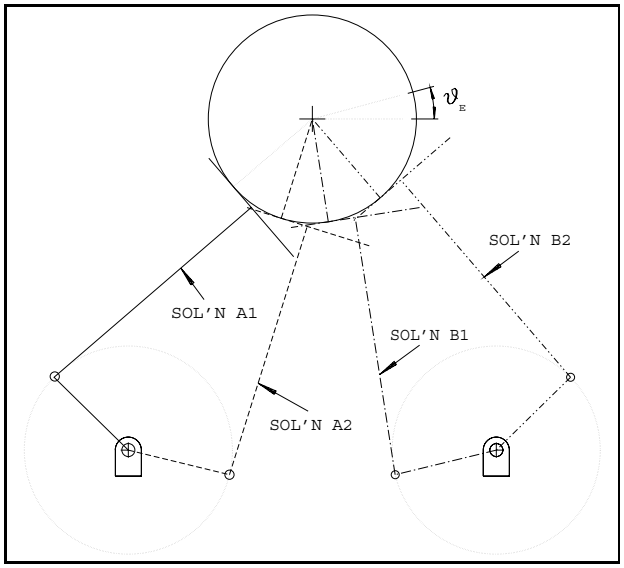

FIGURE 4.2. The solutions for pure rotation from Table 4.1.

occurs, the algorithm requires the calculation of a set of intermediate joint variables. The desired pose array is:

$$\begin{bmatrix} x_E \\ y_E \\ \vartheta_E \end{bmatrix} = \begin{bmatrix} 2.0710 \\ 11.7280 \\ 0^\circ \end{bmatrix}.$$

Sixteen real solutions were obtained. The first four, from Table 4.2 at the end of the chapter, are shown in Fig. 4.3.

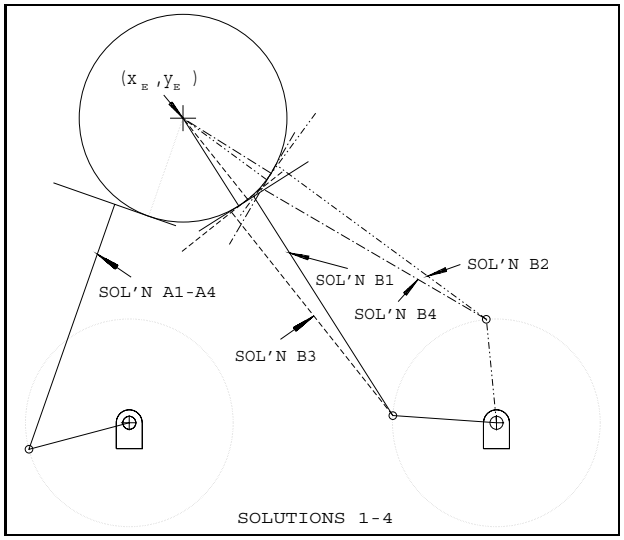

FIGURE 4.3. The first four solutions for pure translation from Table 4.2

EXAMPLE 4.4.3.

General Plane Displacement: The displacements of Examples 4.4.1 and 4.4.2 are combined to give a general plane displacement. The desired pose array is:

$$\begin{bmatrix} x_E \\ y_E \\ \vartheta_E \end{bmatrix} = \begin{bmatrix} 2.0710 \\ 11.7280 \\ 15^\circ \end{bmatrix}.$$

The first four of the sixteen real solutions obtained are illustrated in Fig. 4.4. All sixteen solutions are given in Table 4.3 at the end of the chapter.

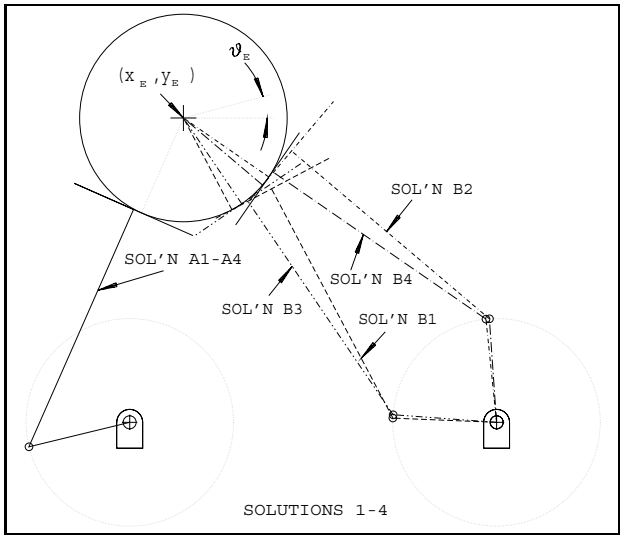

FIGURE 4.4. The first four solutions for general displacement from Table 4.3.

4.5. Tables of Solutions

TABLE 4.1. 4 real solutions for Example 4.4.1.

Sol'n	1	2	3	4
${}^0\vartheta_1^A$ (deg)	135.5602	135.5602	-13.6694	-13.6694
${}^1\vartheta_2^A$ (deg)	265.1628	265.1628	-273.7183	-273.7183
${}^2d_3^A$	1.0472	1.0472	1.0472	1.0472
${}^0\vartheta_1^B$ (deg)	-166.3306	44.4398	-166.3306	44.4398
${}^1\vartheta_2^B$ (deg)	265.1628	-273.7183	265.1628	-273.7183
${}^2d_3^B$	1.0472	1.0472	1.0472	1.0472

TABLE 4.2. 16 real solutions for Example 4.4.2.

Sol'n	1	2	3	4
${}^0\vartheta_1^A$ (deg)	-165.1389	-165.1389	-165.1389	-165.1389
${}^1\vartheta_2^A$ (deg)	235.8174	235.8174	235.8174	235.8174
${}^2d_3^A$	-1.3830	-1.3830	-1.3830	-1.3830
${}^0\vartheta_1^B$ (deg)	176.0545	95.5975	176.1665	95.4856
${}^1\vartheta_2^B$ (deg)	306.3702	-311.9312	312.2698	-305.7674
${}^2d_3^B$	0.6799	0.6799	-0.7953	-0.7953
Sol'n	5	6	7	8
${}^0\vartheta_1^A$ (deg)	-34.8899	-34.8899	-34.8899	-34.8899
${}^1\vartheta_2^A$ (deg)	-224.5344	-224.5344	-224.5344	-224.5344
${}^2d_3^A$	-1.3830	-1.3830	-1.3830	-1.3830
${}^0\vartheta_1^B$ (deg)	176.0545	95.5975	176.1665	95.4856
${}^1\vartheta_2^B$ (deg)	306.3702	-311.9312	312.2698	-305.7674
${}^2d_3^B$	0.6799	0.6799	-0.7953	-0.7953
Sol'n	9	10	11	12
${}^0\vartheta_1^A$ (deg)	-158.0567	-158.0567	-158.0567	-158.0567
${}^1\vartheta_2^A$ (deg)	238.4847	238.4847	238.4847	238.4847
${}^2d_3^A$	-3.5019	-3.5019	-3.5019	-3.5019
${}^0\vartheta_1^B$ (deg)	176.0545	95.5975	176.1665	95.4856
${}^1\vartheta_2^B$ (deg)	306.3702	-311.9312	312.2698	-305.7674
${}^2d_3^B$	0.6799	0.6799	-0.7953	-0.7953
Sol'n	13	14	15	16
${}^0\vartheta_1^A$ (deg)	-41.9721	-41.9721	-41.9721	-41.9721
${}^1\vartheta_2^A$ (deg)	-210.3971	-210.3971	-210.3971	-210.3971
${}^2d_3^A$	-3.5019	-3.5019	-3.5019	-3.5019
${}^0\vartheta_1^B$ (deg)	176.0545	95.5975	176.1665	95.4856
${}^1\vartheta_2^B$ (deg)	306.3702	-311.9312	312.2698	-305.7674
${}^2d_3^B$	0.6799	0.6799	-0.7953	-0.7953

TABLE 4.3. 16 real solutions for Example 4.4.3.

Sol'n	1	2	3	4
${}^0\vartheta_1^A$ (deg)	-166.3263	-166.3263	-166.3263	-166.3263
${}^1\vartheta_2^A$ (deg)	232.5227	232.5227	232.5227	232.5227
${}^2d_3^A$	-0.3358	-0.3358	-0.3358	-0.3358
${}^0\vartheta_1^B$ (deg)	177.6881	93.9640	175.7910	95.8611
${}^1\vartheta_2^B$ (deg)	300.1970	-314.2627	308.4310	-310.4928
${}^2d_3^B$	1.7271	1.7271	0.2519	0.2519
Sol'n	5	6	7	8
${}^0\vartheta_1^A$ (deg)	-33.7025	-33.7025	-33.7025	-33.7025
${}^1\vartheta_2^A$ (deg)	-229.7750	-229.7750	-229.7750	-229.7750
${}^2d_3^A$	-0.3358	-0.3358	-0.3358	-0.3358
${}^0\vartheta_1^B$ (deg)	176.0545	95.5975	175.7910	95.8611
${}^1\vartheta_2^B$ (deg)	300.1970	-314.2627	308.4310	-310.4928
${}^2d_3^B$	1.7271	1.7271	0.2519	0.2519
Sol'n	9	10	11	12
${}^0\vartheta_1^A$ (deg)	-162.3804	-162.3804	-162.3804	-162.3804
${}^1\vartheta_2^A$ (deg)	237.8740	237.8740	237.8740	237.8740
${}^2d_3^A$	-2.4548	-2.4548	-2.4548	-2.4548
${}^0\vartheta_1^B$ (deg)	176.0545	95.5975	175.7910	95.8611
${}^1\vartheta_2^B$ (deg)	300.1970	-314.2627	308.4310	-310.4928
${}^2d_3^B$	1.7271	1.7271	0.2519	0.2519
Sol'n	13	14	15	16
${}^0\vartheta_1^A$ (deg)	-37.6483	-37.6483	-37.6483	-37.6483
${}^1\vartheta_2^A$ (deg)	-217.9837	-217.9837	-217.9837	-217.9837
${}^2d_3^A$	-2.4548	-2.4548	-2.4548	-2.4548
${}^0\vartheta_1^B$ (deg)	176.0545	95.5975	175.7910	95.8611
${}^1\vartheta_2^B$ (deg)	300.1970	-314.2627	308.4310	-310.4928
${}^2d_3^B$	1.7271	1.7271	0.2519	0.2519

Chapter 5

The Forward Kinematics Problem

5.1. The FK Problem Formulation

5.1.1. Difficulties. The FK problem is conventionally expressed as a transformation of the position and orientation of the end effector from a joint space representation to a Cartesian space representation. That is, given a set of n joint variables, one for each n degrees of freedom, determine the position and orientation of the end effector with respect to a non–moving reference coordinate system. The pure rolling nature of the higher pairs makes this manipulator markedly different from planar SG type platforms because the pure rolling condition renders FK solutions completely dependent on the IAC. The FK analysis can not be reduced to the planar SG case because no equivalent mechanism exists which can exactly reproduce a rack–and–pinion motion [**30**]. For this reason, and those discussed in section 4.1 associated with the presence of the higher pairs, the methods in [**54**] and [**21**] can not be used. Hence the FK problem must be reformulated.

5.1.2. Input Variables: Pseudo Inputs. A way to decompose a general displacement of the manipulator to determine the contributions of the racks rolling on the disk and the disk rolling on the racks has proven elusive. As a result, conventional joint variable inputs can not be used. This is because each type of rolling may produce

the same change in the location of the contact point but yields an entirely different displacement. One solution is to modify the problem by using instead a set of *pseudo inputs* from which the position and orientation of the disk in the non–moving reference frame can be determined.

The pseudo inputs are the position of the knee joints in the disk frame, E, as described in section 3.2.6. These positions are

$$\begin{bmatrix} {}^{E}A \\ {}^{E}B \\ {}^{E}C \end{bmatrix}. \tag{5.1.1}$$

Each position is specified by a 2×1 array of Cartesian coordinates expressed in E, hence six pseudo input variables are required. Because the knee joints are constrained to move on circles, the position and orientation of the disk in the non-moving frame Σ can be determined with the kinematic mapping discussed earlier in the same way as [**33, 34**].

The actual joint inputs are the variable joint lengths ${}^{2}d_3^j$, $j \in \{A, B, C\}$. These lengths are the change in distance of the contact point measured along the y_2^j coordinate axis, which is always parallel to the rack. This is why the solution is coupled with the IAC. They are related to the pseudo inputs in the following way:

$$\begin{bmatrix} {}^{T}x_2^j \\ {}^{T}y_2^j \end{bmatrix} = \begin{bmatrix} c^{\Sigma}\phi & -s^{\Sigma}\phi \\ s^{\Sigma}\phi & c^{\Sigma}\phi \end{bmatrix} \begin{bmatrix} {}^{E}x_2^j \\ {}^{E}y_2^j \end{bmatrix}, \tag{5.1.2}$$

$$\begin{bmatrix} {}^{T}x_2^j \\ {}^{T}y_2^j \end{bmatrix} = \begin{bmatrix} (l_2^j + r)c^{\Sigma}\theta_2^j - {}^{2}d_3^j s^{\Sigma}\theta_2^j \\ (l_2^j + r)s^{\Sigma}\theta_2^j + {}^{2}d_3^j c^{\Sigma}\theta_2^j \end{bmatrix}, \tag{5.1.3}$$

where $c \equiv cos$, $s \equiv sin$, and ${}^{\Sigma}\phi$ is the orientation angle of the disk. T is the non–rotating reference frame incident on the origin of E.

Since the reference frame T translates with the disk, ${}^{T}\phi = {}^{\Sigma}\phi$ and, of course, ${}^{T}\vartheta = {}^{\Sigma}\vartheta$. So, the pseudo inputs are theoretically *valid* as input parameters, except that the actual inputs can not be specified until the disk orientation is known. The higher pair variables along with the IAC must be specified or the disk orientation can

not be determined. A cart–before–horse scenario, to be sure. While this approach to the FK problem is not necessarily practical, it is a start. To the best of our knowledge the FK of such a planar parallel platform with higher pairs have never been addressed.

Using the pseudo inputs and IAC, the FK problem of the manipulator shown in Fig. 3.1 can be stated in the following way: Given the coordinates of the three base points A_0, B_0, C_0 in an arbitrary fixed coordinate system, Σ, the coordinates of the knee joints ${}^E A, {}^E B, {}^E C$ expressed in an arbitrary coordinate system, E, which moves with the disk, the fixed lengths of each link, l_i^j, $i \in \{1, 2\}$ and $j \in \{A, B, C\}$, and given the radius of the disk, find the position(s) and orientation(s) of the disk such that the knee joints ${}^E A, {}^E B, {}^E C$ can be joined to the base points A_0, B_0, C_0 with legs of the given lengths.

5.2. Forward Kinematics Algorithm

To obtain the solutions for a given set of inputs, begin by removing the disk connections with legs B and C. Observe that the higher pairs are locked by virtue of the specified input parameter. That is, there can be no relative motion between the disk and the rack because that would change the relative location of the knee joint in the moving coordinate system, E. The knee joint ${}^E A$ is constrained to move on a circle with A_0 as its centre and radius l_1^A. Furthermore, the rigid body comprised of link l_2^A and the disk can rotate about ${}^E A$. Since this is a two parameter motion it must correspond to a two parameter set of points in the image space. This set of image points is a surface, called a *constraint surface*, H. The equation of H is found using equation (2.3.20) and the fact that the moving point ${}^E A$ is bound to a circle. Note that the rack and pinion joints can be actuated by means of power transmission from motors located on the base. The advantages of parallel architecture are contracdicted by placing the motors on the moving platform.

The general homogeneous equation of this circle is determined as follows: A circle with a centre described by the homogeneous coordinates $(X_c : Y_c : Z)$ and radius r has an equation

$$(X - X_c Z)^2 + (Y - Y_c Z)^2 - r^2 Z^2 = 0. \tag{5.2.1}$$

Expanded, this becomes

$$X^2 + Y^2 - 2XX_cZ - 2YY_cZ + X_c^2 Z^2 + Y_c^2 Z^2 - r^2 Z^2 = 0. \tag{5.2.2}$$

We can set

$$\begin{aligned} C_1 &= -X_c, \\ C_2 &= -Y_c, \\ C_3 &= X_c^2 + Y_c^2 - r^2, \end{aligned}$$

and substitute these constants back into equation (5.2.2) to get

$$X^2 + Y^2 + 2C_1XZ + 2C_2YZ + C_3Z^2 = 0. \tag{5.2.3}$$

Recall from Chapter 2 that the equation of the image point (equation (2.3.20)) is given by:

$$\begin{bmatrix} X \\ Y \\ Z \end{bmatrix} = \begin{bmatrix} (X_4^2 - X_3^2) & -2X_3X_4 & 2(X_1X_3 + X_2X_4) \\ 2X_3X_4 & (X_4^2 - X_3^2) & 2(X_2X_3 - X_1X_4) \\ 0 & 0 & (X_4^2 + X_3^2) \end{bmatrix} \begin{bmatrix} x \\ y \\ z \end{bmatrix}. \tag{5.2.4}$$

Substituting the expressions for X, Y, Z from equation (5.2.4) into equation (5.2.3) gives the quadric surface

$$\begin{aligned} H: \quad 0 = {} & z^2(X_1^2 + X_2^2) + (1/4)[(x^2 + y^2) - 2C_1xz - 2C_2yz + C_3z^2]X_3^2 + \\ & (1/4)[(x^2 + y^2) + 2C_1xz + 2C_2yz + C_3z^2]X_4^2 + (C_1z - x)zX_1X_3 + \\ & (C_2z - y)zX_2X_3 - (y + C_2z)zX_1X_4 + (C_1z + x)zX_2X_4 + \\ & (C_2x - C_1y)zX_3X_4. \end{aligned} \tag{5.2.5}$$

It is shown in [**8**] that this quadric constraint surface is a hyperboloid containing the isotropic points $J_1(1 : i : 0 : 0)$ and $J_2(1 : -i : 0 : 0)$. When the other two points

TABLE 5.1. Input parameters.

	${}^{\Sigma}x$	${}^{\Sigma}y$		${}^{E}x$	${}^{E}y$
A_0	0	0	${}^{E}A$	-9	-11
B_0	13	0	${}^{E}B$	9	-11
C_0	10	26	${}^{E}C$	9.5	10.5
$r = 4$	$l_1^j = 4$		$l_1^j = 10$	$j \in \{A, B, C\}$	

B and C are analyzed in turn, three hyperboloidal surfaces are generated, H_A, H_B, and H_C, which correspond to the complete range of possible displacements around the points still connected. The points of intersection of H_A, H_B, and H_C represent the positions of the end–effector where its three knee joints are on their respective circles. Therefore, these points of intersection constitute the solution(s) to the FK problem.

It must be noted that, according to Bézout's theorem [**30**], three second order surfaces can intersect in at most eight points. However, the isotropic points J_1 and J_2 are common to all such constraint hyperboloids, and are therefore always in the solution set. Recall that points with $X_3 = X_4 = 0$ correspond to no real displacement. Since only real solutions are of interest, the isotropic points are discounted. Hence, there are a maximum of six real solutions to the FK problem for manipulators of this type, which confirms the already well known result for planar SG type platforms [**31**].

5.3. Example

EXAMPLE 5.3.1.

5.3.1. Determining the 3 Hyperboloids. Table 5.1 gives the coordinates of the base points A_0, B_0, C_0 in the fixed frame Σ with origin at A_0, the input variable coordinates of the knee joints ${}^{E}A, {}^{E}B, {}^{E}C$ in the moving frame E, with origin at centre of the disk, D, along with the fixed link lengths l_i^j, $i \in \{1, 2\}$, $j \in \{A, B, C\}$ and radius of the disk r.

Substituting the data from Table 5.1 into equation (5.2.5) gives the following three constraint surfaces in the image space:

$$H_A: \quad X_1^2 + X_2^2 + \frac{93}{2}X_3^2 + 46.5X_4^2 + 9X_1X_3 + 11X_2X_3 + 11X_1X_4 - 9X_2X_4 = 0 \tag{5.3.1}$$

$$H_B: \quad X_1^2 + X_2^2 + \frac{589}{4}X_3^2 + \frac{121}{4}X_4^2 - 22X_1X_3 - 4X_2X_4 + 11X_2X_3 + 11X_1X_4 = 0 \tag{5.3.2}$$

$$H_C: \quad X_1^2 + X_2^2 + \frac{3393}{8}X_3^2 + \frac{449}{8}X_4^2 - \frac{39}{2}X_1X_3 - \frac{73}{2}X_2X_3 + \frac{31}{2}X_1X_4 - \frac{1}{2}X_2X_4 - 142X_3X_4 = 0. \tag{5.3.3}$$

These constraint surfaces in the image space are shown from two different perspectives in Fig.'s 5.1 and 5.2. They were generated using Husty's parametrization [**35**]:

$$\begin{bmatrix} X_1 \\ X_2 \\ X_3 \end{bmatrix} = \frac{1}{2}\begin{bmatrix} r\sqrt{s^2+1}\cos t + m \\ r\sqrt{s^2+1}\sin t + n \\ 2s \end{bmatrix},$$

where $m = {}^E y_2^j + C_2 - s(C_1 - {}^E x_2^j)$, $n = s({}^E y_2^j - C_2) - C_1 - {}^E x_2^j$ and $t \in [0, 2\pi]$, $s \in [-\infty, +\infty]$.

Setting the range of parameter s (ie., X_3) to be $[-1, +1]$, the constraint surfaces are clearly seen to be skew hyperboloids in Fig. 5.2. Decreasing this range to $s = -0.1 \rightarrow +0.1$ in Fig. 5.1, the line of intersection between two of the surfaces clearly intersects the third surface in a single point. This single point represents one of the possible six real solutions. The remaining common intersections are not visible because of the display parameters.

5.3.2. Determining the Minimal Univariate Polynomial. Using the Gröbner bases package in the computer algebra software MapleV the equations of the three hyperboloids are easily reduced to a minimal sixth degree univariate polynomial

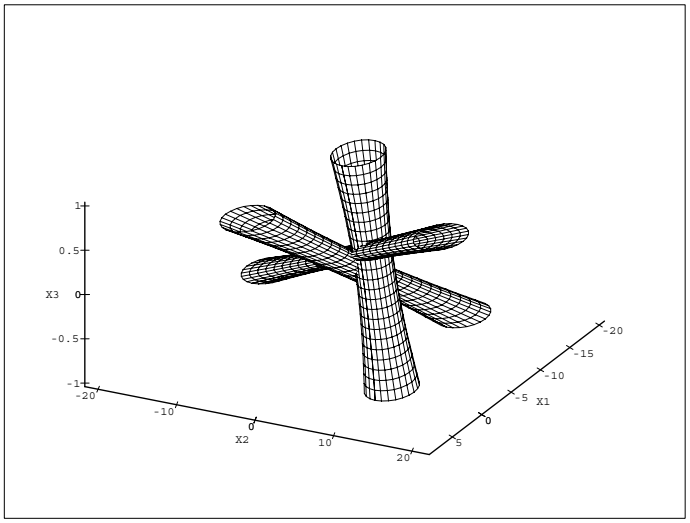

FIGURE 5.1. The constraint surfaces in the image space.

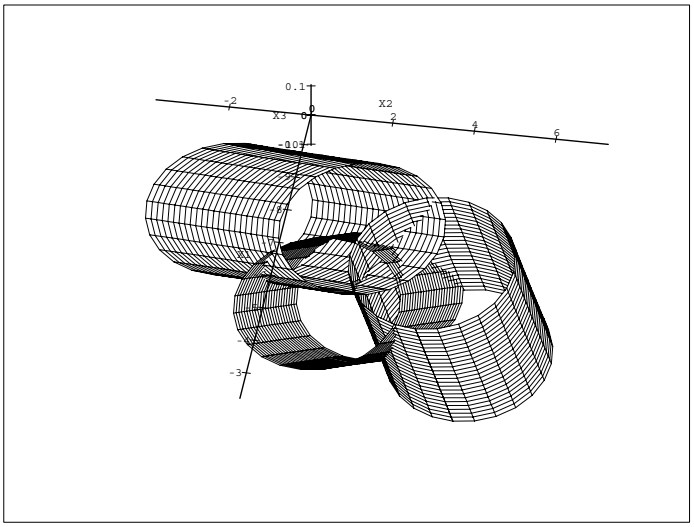

FIGURE 5.2. The range set to $s = -0.1 \rightarrow +0.1$.

in X_3. The default *deglex* ordering was used with $X_1 > X_2 > X_3$. Since X_4 is the homogenising coordinate, its value is arbitrary, hence it is set $X_4 = 1$. The following

reduced Gröbner bases were obtained:

$$
\begin{aligned}
G_1 &= 124X_1X_3 - 403X_3^2 - 20X_2 + 572X_3 + 65 \\
G_2 &= 2945X_2X_3 - 17670X_3^2 - 279X_1 - 242X_2 + 653X_3 - 1523 \\
G_3 &= 11780X_1^2 + 11780X_2^2 + 1669815X_3^2 + 141856X_1 - 78272X_2 - 517792X_3 + \\
&\quad 559207 \\
G_4 &= 11403040X_1X_2 - 35528480X_2^2 - 1418980515X_3^2 - 16692632X_1 - \\
&\quad 208829944X_2 + 83706384X_3 - 204226539 \\
G_5 &= 3161950743325X_3^3 + 14774004800X_2^2 - 11812714672X_1 - 56456371456X_2 + \\
&\quad 191339270949X_3 - 44188577829 \\
G_6 &= 3172473715398785600X_2^3 - 2584472018598685840 0X_2^2 - \\
&\quad 8253732112864254952 5X_3^2 - 3793248184058203348 8X_3 + \\
&\quad 6367252523816862079 2X_2 + 3214412082685214664X_1 \\
&\quad -21984850464217606317
\end{aligned}
$$

This gives six nonlinear equations, some with very large coefficients. However, since these equations represent bases, they are independent, so any three may be used to solve for the three unknowns. The first three bases are selected, as they appear to be the easiest to work with. A univariate polynomial in X_3 is obtained using the elimination method on G_1, G_2, G_3. The resulting polynomial is

$$
\begin{aligned}
&26131824325X_3^6 - 12818984220X_3^5 + 2608119419X_3^4 - 489175320X_3^3 + \\
&88526279X_3^2 - 7719420X_3 + 171025
\end{aligned} \tag{5.3.4}
$$

The roots of this polynomial are then obtained and the set of equations $H_A = 0, H_B = 0, H_C = 0$ can now be solved for the remaining variables X_2, X_3. The

following solutions are obtained:

$$S_1: \quad X_1 = -5.35817508, X_2 = 1.69375244, X_3 = 0.18597447$$

$$S_2: \quad X_1 = -4.23444169, X_2 = 3.13635972, X_3 = 0.15325037$$

$$S_3: \quad X_1 = -4.71288212, X_2 = 2.25800666, X_3 = 0.20703047$$

$$S_4: \quad X_1 = -6.90743973, X_2 = 2.76957064, X_3 = 0.03229377$$

$$S_5: \quad X_1 = -4.306063 + 2.801994i, X_2 = 0.652824 + 0.102659i,$$
$$X_3 = -0.043999 + 0.180029i$$

$$S_6: \quad X_1 = -4.306063 - 2.801994i, X_2 = 0.652824 - 0.102659i,$$
$$X_3 = -0.043999 - 0.180029i$$

There are four real and one set of complex conjugate solutions for a total of six solutions, as expected, since two of the possible eight correspond to J_1 and J_2. Back substitution of the solutions into equations (5.3.1), (5.3.2), and (5.3.3) verifies the four real solutions. The position and orientation of the end–effector corresponding to each of these solutions in terms of the displacement parameters a, b, and ϕ can be found by substituting the solutions for X_1, X_2, X_3, along with $X_4 = 1$ into equations (2.3.21). The subsequent four sets of displacement parameters are given in Table 5.2. The four real solutions are illustrated in Figures 5.3. It is a simple matter of planar Euclidean geometry to determine the the link parameters ${}^2d_3^j$ and ${}^T\theta_2^j$, $j \in \{A, B, C\}$, given the locations of the knee joints in E along with the fixed link lengths and disk radius. These values are given in Table 5.3.

TABLE 5.2. Four real positions and orientations in Σ.

	Sol'n 1	Sol'n 2	Sol'n 3	Sol'n 4
a	1.347918	4.860703	2.459188	5.087701
b	10.967028	9.213788	9.934891	13.979180
ϕ (deg.)	21.070388	17.425626	23.393454	3.699307

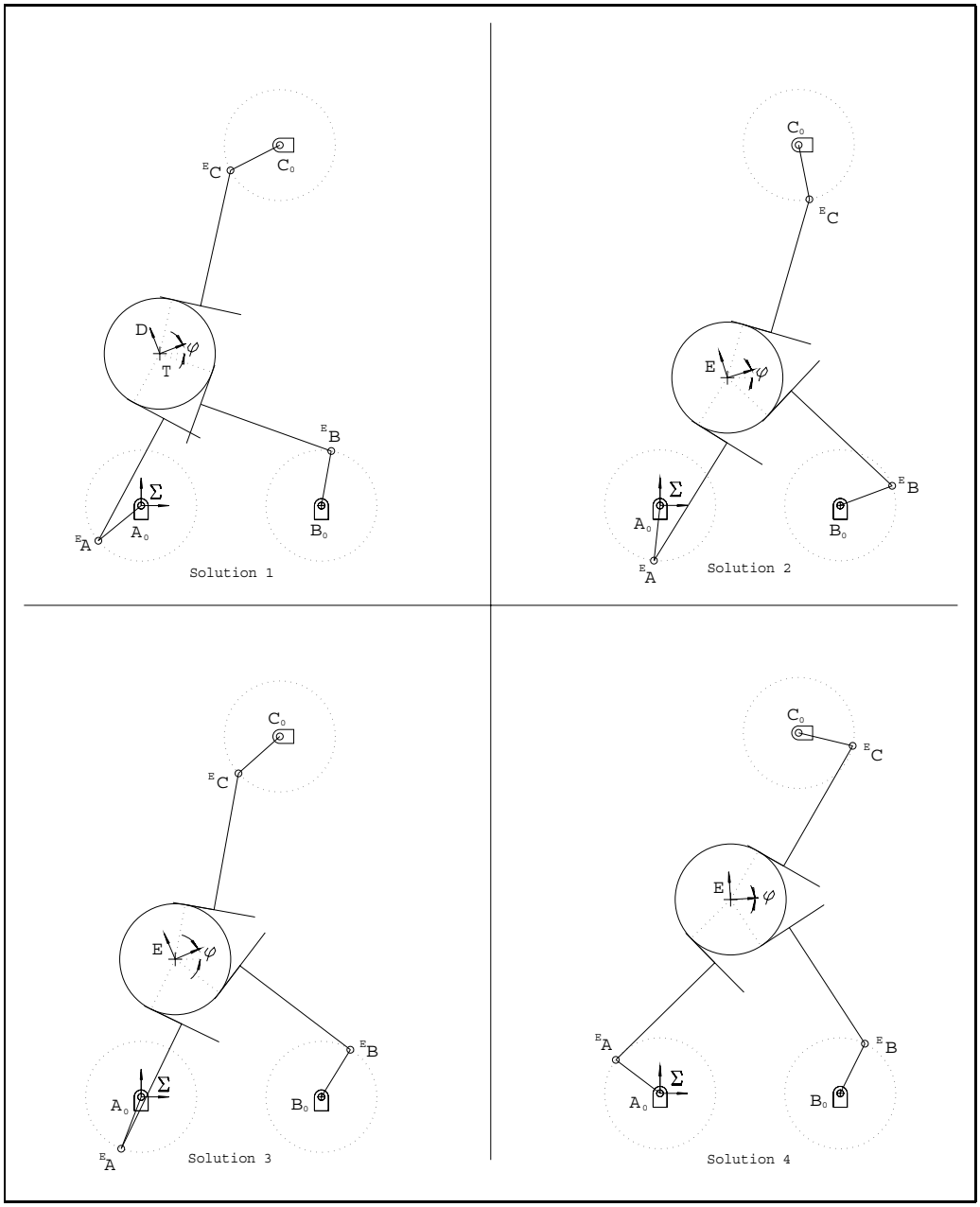

FIGURE 5.3. The four real solutions.

TABLE 5.3. Required joint variable inputs.

	Sol'n 1	Sol'n 2	Sol'n 3	Sol'n 4
${}^2d_3^A$	2.449489	2.449489	2.449489	2.449489
${}^2d_3^B$	-2.449489	2.449489	2.449489	2.449489
${}^2d_3^C$	-2.121320	-2.121320	-2.121320	-2.121320
${}^T\theta_2^A$ (deg.)	241.856762	238.211999	244.179828	224.485681
${}^T\theta_2^B$ (deg.)	-19.715986	-43.209187	-37.241359	-56.935505
${}^T\theta_2^C$ (deg.)	77.548874	73.904112	79.871940	60.177794

Chapter 6

Velocity and Acceleration Analysis

6.1. The Jacobian Matrix

An unconstrained rigid body in the plane has 3 DOF. Suppose we had three functions, each of which depended on the same number of at least three linearly independent variables. These three functions could describe the position and orientation of a planar rigid body in terms of $n \geq 3$ input parameters:

$$y_i \;=\; f_i(x_1, x_2, \ldots, x_n), \quad i \in \{1, 2, 3\}.$$

Employing the chain rule, the differentials of the y_i as functions of the x_n are determined as

$$\delta y_i \;=\; \frac{\partial f_i}{\partial x_1}\delta x_1 + \frac{\partial f_i}{\partial x_2}\delta x_2 + \ldots + \frac{\partial f_i}{\partial x_n}\delta x_n, \quad i \in \{1, 2, 3\}.$$

This result may be expressed more compactly using vector notation as

$$\delta \boldsymbol{Y} \;=\; \frac{\partial \boldsymbol{F}}{\partial \boldsymbol{X}}\delta \boldsymbol{X}. \tag{6.1.1}$$

The $3 \times n$ matrix of partial derivatives, $\frac{\partial \boldsymbol{F}}{\partial \boldsymbol{X}}$, is a linear transformation which maps the δx_n to the δy_i. It is called the *Jacobian matrix*, or simply, the *Jacobian*, and denoted as $\mathbf{J}$. Then the expression in equation (6.1.1) may be rewritten

$$\delta \mathbf{Y} \;=\; \mathbf{J}\delta \mathbf{X}. \tag{6.1.2}$$

Dividing both sides of equation (6.1.2) by the differential time element, δt, $\mathbf{J}$ becomes a mapping of the velocities of $\mathbf{X}$ to the velocities of $\mathbf{Y}$:

$$\dot{\mathbf{Y}} = \mathbf{J}\dot{\mathbf{X}}. \tag{6.1.3}$$

For most robot manipulators the f_i's are non–linear and the partial derivatives are functions of the x_n. Thus, at different instances of time, $\mathbf{J}$ will have different values. The Jacobian, as far as a manipulator is concerned, is a time–varying linear transformation.

The conventional application of $\mathbf{J}$ for serial manipulators is to map joint rates to the Cartesian velocities of the EE, or tip of the arm:

$$\mathbf{V} = \mathbf{J}\dot{\Theta}, \tag{6.1.4}$$

where $\mathbf{V}$ is the vector of Cartesian velocities and $\dot{\Theta}$ is the vector of joint rates. The number of rows in the Jacobian matrix is the same as the number of DOF of the serial manipulator. The number of columns in $\mathbf{J}$ equals the number of joints. For redundant serial manipulators $\mathbf{J}$ is not square: there are more columns than rows. Note that in a serial manipulator all joints must be actuated. A parallel manipulator requires only as many motors as there are DOF. The Jacobian for a parallel manipulator should be constructed, if possible, such that it maps the actuated joint rates to the EE velocities. In this case, the number of rows equals the number of DOF, where as the number of columns equals the number of powered joints.

6.2. Velocity Analysis

The first step in the velocity analysis of the manipulator presented in the previous chapters is to determine the Jacobian matrix for each leg of the manipulator. This can be done by direct differentiation of the kinematic closure equations. From section

4.2 these equations are

$$x_E = l_1^j c_1^j + (l_2^j + r)c_{12}^j - {}^2d_3^j s_{12}^j + l_{0x}^{Ak}, \tag{6.2.1}$$

$$y_E = l_1^j s_1^j + (l_2^j + r)s_{12}^j + {}^2d_3^j c_{12}^j + l_{0y}^{Ak}, \tag{6.2.2}$$

$$\vartheta_E = {}^0\vartheta_1^j + {}^1\vartheta_2^j + \frac{1}{r}({}^2d_3^j - {}^2d_{30}^j) + {}^2\vartheta_{E0}, \tag{6.2.3}$$

where $j = k \in \{A, B, C\}$. The last term in equation (6.2.3) comes from the constraint relation

$${}^2\vartheta_E = \frac{1}{r}({}^2d_3^j - {}^2d_{30}^j) + {}^2\vartheta_{E0}. \tag{6.2.4}$$

Differentiating the closure equations with respect to time gives

$$\dot{x}_E = -l_1^j s_1^j {}^0\dot{\vartheta}_1^j - (l_2^j + r)s_{12}^j({}^0\dot{\vartheta}_1^j + {}^1\dot{\vartheta}_2^j) - {}^2d_3^j c_{12}^j({}^0\dot{\vartheta}_1^j + {}^1\dot{\vartheta}_2^j) - {}^2\dot{d}_3^j s_{12},$$

$$\dot{y}_E = l_1^j c_1^j {}^0\dot{\vartheta}_1^j + (l_2^j + r)c_{12}^j({}^0\dot{\vartheta}_1^j + {}^1\dot{\vartheta}_2^j) - {}^2d_3^j s_{12}^j({}^0\dot{\vartheta}_1^j + {}^1\dot{\vartheta}_2^j) + {}^2\dot{d}_3^j c_{12},$$

$$\dot{\vartheta}_E = {}^0\dot{\vartheta}_1^j + {}^1\dot{\vartheta}_2^j + \frac{1}{r}{}^2\dot{d}_3^j.$$

Collecting terms and expressing the equations in matrix form yields

$$\begin{bmatrix} \dot{x}_E \\ \dot{y}_E \\ \dot{\vartheta}_E \end{bmatrix} = \begin{bmatrix} -(l_1^j s_1^j + l_2^j + r + d_3^j c_{12}^j) & -(l_2^j + r + {}^2d_3^j c_{12}^j) & -s_{12}^j \\ (l_1^j s_1^j + l_2^j + r + d_3^j s_{12}^j) & (l_2^j + r - {}^2d_3^j s_{12}^j) & c_{12}^j \\ 1 & 1 & 1/r \end{bmatrix} \begin{bmatrix} {}^0\dot{\vartheta}_1^j \\ {}^1\dot{\vartheta}_2^j \\ {}^2\dot{d}_3^j \end{bmatrix}.$$

Comparing this last equation with equation (6.1.4), it is seen that the 3×3 matrix which maps the joint rates for a particular leg onto the Cartesian velocities of the disk is the Jacobian for that leg. Hence,

$$\mathbf{J}^j = \begin{bmatrix} -(l_1^j s_1^j + l_2^j + r + d_3^j c_{12}^j) & -(l_2^j + r + {}^2d_3^j c_{12}^j) & -s_{12}^j \\ (l_1^j s_1^j + l_2^j + r + d_3^j s_{12}^j) & (l_2^j + r - {}^2d_3^j s_{12}^j) & c_{12}^j \\ 1 & 1 & 1/r \end{bmatrix}. \tag{6.2.5}$$

Continuing in this fashion, the total Jacobian for the manipulator is a 3×9 matrix. The vector of joint rates, $\dot{\Theta}$, becomes a 9×1 array composed by stacking the three 3×1 joint rate vectors for each leg, $\dot{\Theta}^j$. However, there are only three powered joints, one for each DOF. In this architecture, as described in chapter 5, three motors which control the parameter ${}^2d_3^j$ determine the position and orientation of the disk. Therefore, the rates of change of these parameters set the Cartesian velocities of the

disk. That is, what is needed to produce a desired velocity of the pinion is not all nine joint rates, but only the three ${}^2d_3^j$.

The unactuated joint rates can be eliminated by multiplying both sides of the equation

$$\mathbf{V} \;=\; \mathbf{J}^j\dot{\Theta}^j, \tag{6.2.6}$$

by a 3-dimensional vector $\mathbf{n}$ perpendicular to the first and second columns of $\mathbf{J}^j$. This vector is easily calculated as the cross product of these two columns, namely

$$\mathbf{n} \;\equiv\; \mathbf{j}^{j1} \times \mathbf{j}^{j2}. \tag{6.2.7}$$

The following vector is determined for each leg:

$$\mathbf{n} \;=\; \begin{bmatrix} l_1^j c_1^j \\ l_1^j s_1^j \\ k \end{bmatrix}, \tag{6.2.8}$$

where

$$\begin{aligned} k \;=\; & (l_1^j c_1^j + l_2^j + r - {}^2d_3^j s_{12}^j)(l_2^j + r + {}^2d_3^j c_{12}^j) - \\ & (l_1^j s_1^j + l_2^j + r + {}^2d_3^j c_{12}^j)(l_2^j + r - {}^2d_3^j s_{12}^j). \end{aligned}$$

Multiplication of both sides of equation (6.2.6) by the transpose of $\mathbf{n}$ (i.e., $\mathbf{n}^T$), and then rearranging yields:

$$\begin{aligned} {}^2\dot{d}_3^j \;=\; & r[c_1^j\dot{x}_E + s_1^j\dot{y}_E + \dot{\theta}_E(s_1^j({}^2d_3^j s_{12}^j - l_2^j - r) + \\ & c_1^j({}^2d_3^j c_{12}^j + l_2^j + r))]/[r(s_1^j c_{12}^j - c_1^j s_{12}^j - s_1^j + c_1^j) + \\ & l_2^j(c_1^j - s_1^j) + {}^2d_3^j(s_1^j s_{12}^j + c_1^j c_{12}^j)]. \end{aligned} \tag{6.2.9}$$

Expressions for the joint accelerations can be readily derived by differentiation of the previous equation with respect to time.

6.3. Acceleration Analysis

The dynamics of mechanisms is a field of considerable interest. The dynamics can only be analysed after the kinematic considerations of static position, static force, and velocity. The forces which cause the motion of a manipulator are typically analysed using the Newton–Euler, Lagrange, or Kane's method. The Newton–Euler approach requires the immediate calculation of the manipulator accelerations.

The relationship between the Cartesian and joint accelerations is derived by the differentiation of equation 6.1.4 with respect to time, giving

$$\dot{\mathbf{V}} = \dot{\mathbf{J}}\dot{\Theta} + \mathbf{J}\ddot{\Theta}. \tag{6.3.1}$$

Alternately, expressions for the joint accelerations can be readily derived by differentiation of equation (6.2.9) with respect to time.

Chapter 7

Concluding Remarks

7.1. Conclusions

This thesis has presented a kinematic analysis of a planar parallel manipulator with holonomic higher pairs. This analysis involved the detailed investigation of the IK and FK position problems, and a cursory look at the velocity and acceleration analysis.

As a prelude to the study, the relevant geometry and mathematics were reviewed. The group of planar isometries and the group properties proved to be important for the development of the IK algorithm. Specifically, planar displacements are decomposable into components of certain translations and rotations, and these components commute. Kinematic mapping and Gröbner bases theory were discussed in detail. They proved to be useful and elegant tools for the FK problem.

After describing the manipulator, a mobility analysis was performed. Furthermore, six special geometric properties were observed which proved to be useful in developing the IK algorithm.

An algorithm for determining closed form analytical solutions to the IK problem was developed. Because the algorithm proceeds on a leg–by–leg basis, solutions can be obtained for similar rolling systems comprised of any number of 2R serial legs. It

turns out that the upper bound on the number of real solutions for any such system is 4^n, where n is the number of 2R legs.

Husty's FK algorithm was adapted for the holonomic higher pairs by the introduction of pseudo inputs to be used as powered joint inputs for the FK problem. The kinematic mapping approach yields promising results for this initial effort with the exception of a small direction anomaly. The anomaly is probably due to the problem formulation using the pseudo inputs. It is believed that this may be overcome with minor correction of the algorithm. In any event, the procedure needs reformulation because of the fact that the real inputs can not be specified from the pseudo inputs alone, but require knowledge of the actual disk orientation. The FK solutions in the example were easily obtained using Gröbner bases.

Finally, the Jacobian for the manipulator was determined. It was then used in a velocity and acceleration analysis.

7.2. Suggestions for Future Research

The workspace singularity analysis in chapter 6 appears to hold the promise of great interest. Based on this preliminary work, it would appear that the interior of the workspace is devoid of singularities. If this is so, then the manipulator has a bright future. Hence, it is recommended that a detailed workspace and singularity analysis be carried out. The manipulator dynamics should also be investigated. Since the Jacobian matrices are known, the Newton–Euler method could be used.

For practical design reasons, the IK and FK solutions must be made quickly available to the controller or path planner. The FK problem needs to be reformulated to eliminate the direction ambiguity which is, apparently, generated by the use of the pseudo inputs. Better still, the problem should be reformulated to allow the actual powered joint variables to be used as inputs.

Once a better formulation of the FK problem exists, manipulator motions should be simulated. The animation should expose any flaws in the IK and FK solution procedures. Then issues of obstacle avoidance and trajectory planning can be addressed. After these tasks have been completed, the design of a prototype should commence. With a sound design in place, the construction of a prototype should be considered.

REFERENCES

[1] Adams, W., Loustaunau, P., 1994, *An Introduction to Gröbner Bases*, American Mathematical Society, Graduate Studies in Mathematics, Vol. 3.

[2] Angeles, J., 1988, *Rational Kinematics*, Springer Tracts in Natural Philosophy, Springer-Verlag, New York, N.Y..

[3] Agrawal, S.K., Pandravada, R., 1992, "Inverse Kinematic Solutions of a Rolling Disk Between Two Planar Manipulators", *Robotics, Spatial Mechanisms, and Mechanical Systems, ASME*, DE-Vol. 45, pp. 473-478.

[4] Agrawal, S.K., Pandravada, R., 1993, "Kinematics and Workspace of a Rolling Disk Between Planar Manipulators", *Proc. Am. Control Conf.*, San Francisco, Cal., pp. 741-745.

[5] Ayres, F., 1967, *Projective Geometry*, Schaum's Outline Series in Mathematics, McGraw–Hill Book Company, New York, N.Y..

[6] Becker, T., Weispfenning, V., 1993, *A Computational Approach to Commutative Algebra*, Graduate Texts In Mathematics, Springer–Verlag, New York, N.Y..

[7] Biggs, N.L., 1989, *Discrete Mathematics*, revised edition, Clarendon Press, Oxford, England.

[8] Bottema, O., Roth, B., 1979, *Theoretical Kinematics*, Dover Publications, Inc., New York, N.Y..

[9] Bumcrot, R.J., 1969, *Modern Projective Geometry*, Holt, Rinehart & Winston, Inc., New York, N.Y..

[10] Chen, H., 1991, *Kinematics and Introduction to Dynamics of a Movable Pair of Tetrahedra*, M.Eng thesis, Dept. of Mech. Eng., McGill University, Montréal, Canada.

[11] Clark, A., 1971, *Elements of Abstract Algebra*, Dover Publications, Inc., New York, N.Y..

[12] Cole, A., Hauser, J., Sastry, S., 1988, "Kinematics and Control of Multifingered Hands with Rolling Contact", *Proc. of IEEE Int. Conf. Rob. Aut.*, pp. 228-233.

[13] Coxeter, H.S.M., 1954, *The Real Projective Plane*, second edition, Cambridge At The University Press, England.

[14] Coxeter, H.S.M., 1969, *Introduction to Geometry*, second edition, John Wiley & Sons, Inc., Toronto, Canada.

[15] Coxeter, H.S.M., 1974, *Projective Geometry*, second edition, University of Toronto Press, Toronto, Canada.

[16] Craig, J.J., 1989, *Introduction to Robotics, Mechanics and Control*, second edition, Addison-Wesley Publishing Co., Reading, Mass..

[17] Denavit, J., Hartenberg, R.S., June 1955, "A Kinematic Notation for Lower-Pair Mechanisms Based on Matrices", *J. of Applied Mechanics*, pp. 215-221.

[18] Dolciani, P., Berman, S., Wooton, W., 1963, *Modern Algebra and Trigonometry*, Thomas Nelson & Sons (Canada) Ltd., Don Mills, Ontario, Canada.

[19] Fichter, E.F., June 1988, "A Stewart Platform–Based Manipulator: General Theory and Practical Construction", *J. Robotics Research*, Vol. 5, No. 3, pp. 354-360.

[20] Gosselin, C., 1988, *Kinematic Analysis, Optimization and Programming of Parallel Robotic Manipulators*, Ph.D. thesis, Dept. of Mech. Eng., McGill University, Montréal, Canada.

[21] Gosselin, C., Sefrioui, J., 1991, " Polynomial Solutions For the Direct Kinematic Problem of Planar Three–Degree–of Freedom Parallel Manipulators", *Proc. 5th Int. Conf. on Adv. Rob. (ICAR)*, Pisa, Italy, pp. 1124–1129.

[22] Gosselin, C., Sefrioui, J., Richard, M., 1992, "On The Direct Kinematics of General Spherical Three–Degree–of–Freedom Parallel Manipulators", *Robotics, Spatial Mechanisms, and Mechanical Systems, ASME*, DE–Vol. 45, pp. 7-11.

[23] Gough, V.E., 1956, "Discussion in London: Automobile Stability, Control, and Tyre Performance", *Proc. Automobile Division, Institution of Mech. Engrs.*, pp. 392–394.

[24] Harris, J., 1992, *Algebraic Geometry*, Graduate Texts In Mathematics, Springer–Verlag, New York, N.Y..

[25] Harms, E., Kounias, S., Vroomen, L., Zsombor–Murray, P., 1991, "A Binary–Decision/Transputer Network For The Control of a Planar Three Drgree of Freedom Parallel Robotic Manipulator", *Microprocessing and Microprogramming, North–Holland*, pp 137–142.

[26] Hartenberg, R.S., Denavit, J., 1964, *Kinematic Synthesis of Linkages*, McGraw-Hill, Book Co., New York, N.Y..

[27] Hayes, M.J.D., Zsombor–Murray, P., 1996, "A Planar Parallel Manipulator with Holonomic Higher Pairs: Inverse Kinematics", *Proc. CSME Forum 1996, Symposium on the Theory of Machines and Mechanisms*, Hamilton, Ont., Canada., pp. 109–116.

[28] Hayes, M.J.D., Zsombor–Murray, P., 1996, "Kinematic Mapping of 3–legged Planar Platforms With Holonomic Higher Pairs ", *Recent Advances in Robotic Kinematics*, eds. Lenarčič, J., Parenti–Castelli, V., Kluwer Academic Publishers, Dordrecht, pp. 421–430.

[29] Hilbert, D., Cohn–Vossen, S., 1932, Anschauliche Geometrie, English translation 1990 by Nemenyi, P.: *Geometry and The Imagination*, Chelsea Publishing Company, New York, N.Y..

[30] Hunt, K.H., 1978, *Kinematic Geometry of Mechanisms*, Clarendon Press, Oxford, England.

[31] Hunt, K.H., 1983, "Structural Kinematics of In–Parallel–Actuated robot arms", *ASME J. of Mech., Trans. and Automation in Design*, Vol. 105, No. 4, pp. 705–712.

[32] Hunt, K.H., Primrose, E.J.F., 1993, "Assembly Configurations of Some In-Parallel-Actuated Manipulators", *Mech. Mach. Theory*, Vol. 28, No. 1, pp. 31-42.

[33] Husty, M.L., 1994, "An Algorithm for Solving the Direct Kinematics of Stewart–Gough–Type Platforms", Internal Report, Mcgill, Centre for Intelligent Machines, CIM-94-07.

[34] Husty, M.L., 1995, "Kinematic Mapping of Planar Three–Legged Platforms", Proc. *15th Canadian Congress of Applied Mechanics (CANCAM 1995)*, Victoria, B.C., Canada, Vol. 2, pp. 876-877.

[35] Husty, M.L., May 1996, "On The Workspace of Planar Three–legged Platforms", to appear in *Proc. World Automation Conf., 6th Int. Symposium on Rob. and Manuf. (ISRAM 1996)*, Montpellier, France.

[36] Husty, M., Zsombor-Murray, P., 1994, "A Special Type of Singular Stewart–Gough Platform", *Advances in Robot Kinematics and Computational Geometry*, eds. Lenarčič, J. and Ravani, B., Kluwer Academic Publishers, Dordrecht, pp. 449-458.

[37] Karger, A., Husty, M.L., 1996, "On Self Motions of a Class of Parallel Manipulators", *Recent Advances in Robotic Kinematics*, eds. Lenarčič, J., Parenti–Castelli, V., Kluwer Academic Publishers, Dordrecht, pp 339–348.

[38] Lee, K.M., Saha, D.K., 1987, "Kinematic Analysis of a Three Degree of Freedom In–Parallel Actuated Manipulator", *Proc. IEEE Conf. on Robotics and Automation*, pp. 345-350.

[39] McCarthy, J.M., 1990, *An Introduction to Theoretical Kinematics*, The M.I.T. Press, Cambridge, Massachusetts.

[40] Mimura, N., Funahashi, Y., 1992, "Kinematics of Planar Multifingered Robot Hand with Displacement of Contact Points", *JSME International Journal*, Series 3, Vol. 35, No. 3, pp. 462-469.

[41] O'Neill, B., 1966, "Elementary Differential Geometry", Academic Press, Inc., Boston, Massachusetts.

[42] Paul, B., 1979, Kinematics and Dynamics of Planar Machinery, Prentice–Hall, Inc., N.J..

[43] Ravani, B., Roth, B., Sept. 1983, "Motion Synthesis Using Kinematic Mappings", ASME, *J. of Mechanisms, Transmissions, & Automation in Design*, Vol. 105, pp. 460-467.

[44] Roth, B., 1993, "Computations in Kinematics", in *Computational Kinematics*, eds. Angeles, J., Hommel, G., Kovács, P., Kluwer Academic Publishers, Dordrecht, pp. 3-14.

[45] Roth, B., 1994, "Computational Advances in Robot Kinematics", in *Advances in Robot Kinematics and Computational Geometry*, eds. Lenarčič, J. and Ravani, B., Kluwer Academic Publishers, Dordrecht, pp. 7-16.

[46] De Sa, S., Roth, B., July 1981, "Kinematic Mappings. Part 1: Classification of Algebraic Motions in the Plane", *ASME, J. of Mech. Design*, Vol. 103, pp. 585-591.

[47] De Sa, S., Roth, B., Oct. 1981, "Kinematic Mappings. Part 2: Rational Algebraic Motions in the Plane", *ASME, J. of Mech. Design*, Vol. 103, pp. 712-717.

[48] Sachs, H., et. al., 1993, *Comett II, Modul II: Linengeometrie*, Manuscript, Graz, Austria.

[49] Saha, S.K., Angeles, J., May 1989, "Kinematics and Dynamics of 3-wheeled 2-DOF AGV", *Proc. of IEEE Int. Conf. Rob. Aut*, Scottsdale, Ariz., pp. 1572-1577.

[50] Saha, S.K., Angeles, J., March 1991, "Dynamics of Nonholonomic Mechanical Systems Using a Natural Orthogonal Compliment", *J. of Applied Mechanics, ASME*, Vol. 58, pp. 238-243.

[51] Salisbury, J.K., Roth, B., March 1983, "Kinematic and Force Analysis of Articulated Mechanical Hands", *J. of Mech., Trans., and Aut. in Design, ASME*, Vol. 105, pp. 35-41.

[52] Sommerville, D.M.Y., 1934, *Analytical Geometry of Three Dimensions*, Cambridge University Press, London, England.

[53] Stewart, D., 1965, "A Platform With Six Degrees of Freedom", *Proc. Instn. Mech. Engr.*, Vol. 180, Part 1, No. 15, pp. 371-378.

[54] Wohlhart, K., March 1992, "Direct Kinematic Solution of the General Planar Stewart Platform", *Proc. of the Int. Conf. on Computer Integrated Manufacturing*, Zakopane, Poland, pp. 403–411.

[55] Yun, X., Kumar, V., Sarkar, N., Paljug, E., May 1992, "Control of Multiple Arms with Rolling Constraints", *Proc. of IEEE Int. Conf. Rob. Aut.*, Nice, France, pp. 2193-2198.

[56] Zsombor-Murray, P.J., Hyder, A., 1992, "An Equilateral Tetrahedral Mechanism", *Robotics and Autonomous Systems*, pp. 227-236.

[57] Zsombor-Murrary, P., J. & Husty, M.L., June 1994, "Engineering Graphics, Computational Geometry and Geometric Thinking", *Proc of ASEE Annual Conf.*, Edmonton, Canada, Vol. 1, pp. 437-443.

Appendix A

Geometry of The Image Space

A.1. Erlangen Programme

In 1872, F. Klein introduced his *Erlangen Programme* as a means of classifying geometries according to the groups of transformations which leave the propositions intact. Usually these groups have sub–groups that preserve the central concepts of the geometry [**13**].

The Erlangen Programme is conveniently stated in the form of three propositions [**46**]:

Proposition 1: A geometry on a space defines a group of transformations in that space.

Proposition 2: A group of transformations in a space defines a geometry on that space.

Proposition 3: Geometry is the study of those relations which remain invariant under the group of transformations associated with it.

In Euclidean geometry the group of isometries preserves distance and angle. The isometries are actually a sub–group of the similarity transformations. It is this group which preserves the propositions of Euclidean geometry [**15**].

Projective geometry does not admit concepts of length, angle, parallelism, or betweenness, and hence, is different from Euclidean geometry. Indeed, using the Erlangen Programme, projective geometry is classified by the group of *collineations* and *correlations*. These groups preserve the class of points and the class of lines [**13, 9**].

A collineation is a point–to–point correspondence which preserves collinearity. A planar correlation is a point–to–line, or line–to–point correspondence relating collinear points to concurrent lines.

A.2. Image Space Geometry

Following the propositions of Klein's Erlangen Programme, the image space group and its invariants may be determined for the mapping given by equation (2.3.13). Hence, the geometry on the image space may be defined. A very detailed investigation is given in [**8**], and the results were used in [**46**] to classify planar algebraic motions.

The image of a displacement given by the three parameters (a, b, ϕ) is dependent on the arbitrary zero positions of the reference frames E and Σ. Therefore, there are ∞^6 mappings. It is shown in [**8**] that if $(X_1 : X_2 : X_3 : X_4)$ is a representation of a displacement all other allowable representations $(X_1' : X_2' : X_3' : X_4')$ are related to it by

$$X_i' = \sum_{i=1}^{4} \sum_{j=1}^{4} c_{ij} X_j, \tag{A.2.1}$$

where the c_{ij} obey

$$\begin{aligned} c_{11} &= c_{22}, \\ c_{12} &= -c_{21}, \\ c_{33} &= c_{44}, \\ c_{34} &= -c_{43}, \\ c_{11}c_{22} - c_{12}c_{21} &= c_{33}c_{44} - c_{34}c_{43}, \\ c_{31} = c_{32} &= c_{41} = c_{42} = 0. \end{aligned} \tag{A.2.2}$$

Equations (A.2.1) and (A.2.2) represent a group G of ∞^6 non–singular linear transformations in Σ' connecting all the allowable representations of a given displacement [**46**]. The group G of transformations and its invariants determines the Σ' geometry. G has six independent parameters and five invariants. The invariants are [**8**]:

(i) The line $l(X_3 = X_4 = 0)$.

(ii) The isotropic points $J_1(1 : i : 0 : 0)$ and $J_2(1 : -i : 0 : 0)$ on the line l.

(iii) The conjugate imaginary planes $V_1(X_3 = iX_4)$ and $V_2(X_3 = -iX_4)$.

The *isotropic* points refer to the intersection points of a line which cuts the circle at infinity [**52**].

The invariant elements in the non–Euclidean hyperbolic and elliptic geometries are respectively, general real and imaginary quadrics. Whereas, in the Σ' geometry they consist of two imaginary planes. As a result, the geometry on the image space of the mapping is identical with none of the classical metric geometries. In [**8**] the Σ' geometry is labelled *quasi–elliptic*, since it is considered a borderline case of elliptic geometry. Furthermore, the metric concepts of the distance between two points, the angle between two planes, and the parallelism of two lines are defined. Finally,

it is shown that two sets of transformations in Σ' are comparable to rotations and translations of Euclidean geometry.

Of interest are three special cases [**35**]:

(i) $X_3 = 0, X_4 \neq 0 \Rightarrow \phi = 0$: These are the pure translations in the Euclidean plane.

(ii) $X_3 \neq 0, X_4 = 0 \Rightarrow \phi = \pi$: These are the 180° half–turns in the Euclidean plane.

(iii) $X_3 =$ constant, $\Rightarrow X_4 =$ constant: This situation corresponds to translations in the Euclidean plane where the moving frame E maintains a constant angle with respect to the fixed frame Σ.

Document Log:

Manuscript Version 1

Typeset by $\mathcal{AMS}$-LaTeX — 1 May 2000

Matthew John D. Hayes

Center for Intelligent Machines, McGill University, 3480 University St., Montréal (Québec) H3A 2A7, Canada, *Tel.* : (514) 398-3938

E-mail address: johnh@cim.mcgill.ca